Surface rupture of the Hundalee Fault during the M_W7.8 2016 Kaikōura Earthquake

Jack N Williams*, David J A Barrell, Mark W Stirling, Katrina M Sauer, Grace C Duke, Ken X Hao

*Corresponding author: williamsj132@cardiff.ac.uk

Otago Earthquake Science Group, Department of Geology, University of Otago, PO Box 56, Dunedin 9054, New Zealand

Abstract

The Hundalee Fault is one of at least 20 faults that ruptured during the M_W7.8 2016 Kaikōura Earthquake in the northeast of the South Island of New Zealand. Here, we document a 12 km onshore section of the Hundalee Fault that exhibited surface rupture from this event. To the northeast of our observations, the fault crosses the coast and independent seabed surveys show the 2016 rupture continued at least 2 km offshore. No surface rupture was observed across the southwestern section of the Hundalee Fault, which crosses hilly vegetated terrain and poorly consolidated valley-floor sediment. However, previous InSAR analyses suggests that a 9 km length section of the fault did rupture. Hence, the minimum length of the 2016 rupture along the Hundalee Fault is 23 km. Field measurements indicate oblique dextral-reverse slip along northeast trending Hundalee Fault sections and reverse-sinistral slip along north to north-northeast trending sections. This is consistent with the regional principal horizontal shortening direction. Maximum vertical and horizontal offset measurements are 2.5 ± 0.5 m and 3.7 ± 0.5 m respectively. The discontinuous and irregular surface ruptures we observed are characteristic of a structurally immature fault. Yet, previous geological mapping indicates that the Hundalee Fault is a regionally significant fault with >1 km late Cenozoic throw. Furthermore, a 60 m wide sequence of fault rocks exposed by the rupture indicates that slip has localized into <10 cm thick gouge zones, as anticipated for a mature fault. Therefore, a discrepancy exists between geological evidence of the Hundalee Fault being a structurally mature fault and the characteristics of the 2016 rupture. We speculate that this signifies that the 2016 rupture was imposed on the Hundalee Fault by movement across an inefficient multi-fault network rather than independent rupture of the Hundalee Fault itself.

Introduction

The M_W7.8 Kaikōura Earthquake, at local time 00:03 hours on the 14 November 2016 (11:03 13 November UTC) in the northeast of the South Island of New Zealand, produced surface rupture on a multitude of faults (Fig. 1; Hamling et al., 2017; Stirling et al., 2017; Litchfield et al., 2018). Collectively, these faults exhibit considerable diversity in length, maturity, slip rates, and slip senses, and transect two adjoining tectonic domains (Fig. 1; Stirling et al., 2012; Litchfield et al., 2014a). This paper investigates the Hundalee Fault, which lies at the southeastern margin of the Kaikōura Earthquake fault surface rupture zone.

The northeast striking Hundalee Fault was well known prior to the earthquake, being a clearly defined structural dislocation within bedrock geological units (Fig. 2; Warren, 1995; Rattenbury et al., 2006; Heron, 2014). No fault-specific paleoseismic investigations have been done on the Hundalee Fault to date, and prior to the earthquake there were no unambiguous Quaternary-age landform offsets documented along the mapped trace of the fault. Accordingly, its slip rate and recurrence interval are poorly constrained (Barrell and Townsend, 2012; Barrell, 2015). Nevertheless, it was presumed to be an active fault (Pettinga et al., 2001; Barrell and Townsend, 2012; Litchfield et al., 2014a; Langridge et al., 2016) and was included as an earthquake source in the 2010 New Zealand National Seismic Hazard Model (Stirling et al., 2012). Herein, we document the surface rupture characteristics generated by the Kaikōura Earthquake along the Hundalee Fault (Fig. 1). In doing so, we also focus on reconciling an apparent dichotomy between our fault rupture observations and the longer-term behavior of the fault.

Tectonic setting of the Kaikōura Earthquake and the Hundalee Fault

The 2016 M_W7.8 Kaikōura Earthquake occurred where motion between the Pacific and Australian plates transitions from the Hikurangi subduction zone to oblique continental collision (Fig. 1; e.g. Wallace et al., 2012; Hamling et al., 2017). The Hundalee Fault is one of a number of other northeast striking reverse and transpressional faults that constitute the relatively low strain (2.3 ± 0.7 mm/yr cumulative net slip rate) North Canterbury tectonic domain (NCD; Litchfield et al., 2014a). To the north of the NCD, lies an array of major dextral strike-slip faults that constitute the Marlborough Fault System (MFS). The Kaikōura earthquake initiated in the NCD (Kaiser et al, 2017; Nicol et al., 2018), where it ruptured at least five faults, before it propagated to the northeast across several different faults within the MFS (Fig. 1; Hamling et al., 2017, Litchfield et al., 2018; Kearse et al., 2018).

Geological setting of the Hundalee Fault

The regional geology surrounding the Hundalee Fault comprises a basement of Mesozoic-age greywacke and associated rocks (Torlesse Supergroup). Overlying this is a Late Cretaceous to Early Pleistocene largely marine transgressive-regressive sedimentary sequence. Maximum regional submergence occurred in the Oligocene when the Amuri Limestone, a regionally important stratigraphic marker, was deposited (Warren, 1995; Rattenbury et al., 2006). In places, poorly consolidated surficial sediments of Pleistocene to Holocene age cap this sequence (Fig. 2).

Based on interpretations of geological relationships, Warren (1995) showed the Hundalee Fault having an onshore length of ~30 km (Fig. 2; Warren, 1995). The fault has also been extrapolated offshore to the northeast by between 10 km (Barrell, 2015) to 25 km (Litchfield et al., 2014a). At Te Moto Moto Stream, Amuri Limestone outcrops at ~40 m above sea level (asl) on the downthrown (southeastern) side of the fault (Fig. 2). On the upthrown northwest side of the fault, Torlesse basement forms mountain terrain, with peak heights as much as 800 m asl. The structural position of the Amuri Limestone is ~0.5 km above the top of Torlesse basement in this area (Warren, 1995), implying a minimum Late Cenozoic vertical separation (throw) of 1.2 km across the Hundalee Fault at this location.

There are stratigraphic considerations relevant to the evolution of the Hundalee Fault. By the mid-Pliocene (3.5 Ma), the area around the fault had undergone a major episode of differential tectonic movement (Warren, 1995). This is highlighted in the Leader basin (Fig. 2), where the mid-Miocene to Early Pleistocene marine to marginal marine Greta Formation is as much as 1.5 km thick (Warren 1995). This contrasts with a more typical ~500 m thickness of this formation elsewhere in the region (Rattenbury et al., 2006). Southeast of the Hundalee Fault, the stratigraphic record demonstrates localized uplift, the concomitant erosional removal of a ~1 km thick blanket of Late Cretaceous to early Miocene sedimentary rocks, and the deposition of mid-Pliocene marine conglomeratic facies of the Greta Formation directly on Torlesse basement rocks (Warren, 1995).

These considerations bear upon the interpretation of the southwestern sector of the Hundalee Fault. We suggest that Warren's (1995) depiction of the Leader basin on the upthrown (southeast) side of the Hundalee Fault is possibly incorrect as the sense of throw is wrong. Instead, it is noted that there is a moderately northwest-dipping sequence of the Late Cretaceous-Oligocene strata to the northeast of Ferniehurst (Fig. 2), but Pliocene Greta Formation is mapped immediately to the east in the floor of the Conway River valley (Warren, 1995). This juxtaposition of strata implies the need for a fault with several hundred meters of upthrow to the northwest. A simple explanation is that this structure is the true position of the southern part of the Hundalee Fault, about 1 km east of where it is depicted on published maps (Fig. 2). Whether the fault dies out in this area or continues farther southwest into the area of smaller faults mapped by Warren (1995) is unknown.

In places northeast of the Conway River, Warren (1995) mapped the Hundalee Fault as concealed under the Greta Formation, implying that the fault has not moved since the deposition of that stratigraphic unit. This is incorrect in detail because there is good evidence for previous Late Quaternary surface rupture as documented later in this paper. However, it is not currently possible to quantify the amount of Late Cenozoic throw on the Hundalee Fault that had been accrued prior to or during the deposition of the Greta Formation.

Mapping and documentation methods

Surface rupture that occurred on the Hundalee Fault during the Kaikōura Earthquake was recognized quickly after the event, on account of its multi-meter oblique dextral-reverse offset of State Highway 1 (SH1) and the South Island Main Trunk Railway (SIMT) at the coast (Fig. 3). We undertook ground-based mapping and documentation of the surface ruptures in two trips, one and six weeks after the earthquake (21-24 November and 19-21 December 2016). Helicopter reconnaissance along the Hundalee Fault, and the adjacent Stone Jug and Whites faults (Litchfield et al., 2018) was undertaken on 19 December.

Surface ruptures were mapped using handheld and Real Time Kinetic (RTK) global positioning system (GPS) survey equipment (Fig. S1, available in the electronic supplement to this article). Rupture mapping was assisted by recourse to InSAR images (Hamling et al., 2017), aerial photographs, geological mapping of the Hundalee Fault (Warren, 1995; Rattenbury et al., 2006; Barrell and Townsend, 2012), and lidar surveys collected with 2-4 weeks of the earthquake (Fig. S2, available in the electronic supplement to this article), from which digital elevation models (DEMs) with sub-meter resolution were generated (Clark et al., 2017; Litchfield et al., 2018).

Hundalee Fault surface ruptures typically offset linear features in an oblique manner. For discrete and mostly linear features, such as stream terrace risers, road lines, fences, and vehicle tracks, or point features such as sheared off tree roots, we visually reconstructed the offset in the near-field (i.e. within a few meters of the rupture trace). We did this by projecting the displaced feature into the fault and then measuring the horizontal component (if any) parallel to the strike of the rupture trace. For the vertical component, which generally was measured with reference to the ground surface, we projected natural ground slopes into the fault and measured the vertical offset. Measurements were made using a handheld tape measure and for sloping surfaces a clinometer was also employed to aid in our projections. A representative uncertainty for each measurement site was assigned based on our qualitative best estimate of the precision with which each feature could be reconstructed (Litchfield et al., 2014b). We assigned low uncertainties (± 0.1 m) for discrete features running at a high angle to the surface rupture (e.g. fences, vehicle tracks), while features that were more subtle (e.g. scarp height, stream beds) or were oblique to the surface rupture were assigned higher uncertainties (more than ± 0.2 m).

Wherever possible we subsequently reviewed the field measurements using RTK data (Fig. S1, available in the electronic supplement to this article), post-earthquake aerial photographs, and lidar datasets (Fig. S2, available in the electronic supplement to this article). In some cases, the lidar or RTK data enabled us to make a far-field estimate of the vertical component of movement (Fig. S1 and S2, available in the electronic supplement to this article). Furthermore, in some localized areas of pre-earthquake (2012) lidar acquisition, we could determine the vertical deformation by subtracting the 2012 model from the 2016 model, as described by Clark et al., (2017). In most places the amount of lateral motion was sufficiently small, so that ground surfaces of different elevation were not brought side by side. Therefore, the difference between the two models is closely representative of the true coseismic vertical displacement (Clark et al., 2017).

A DJI Phantom Professional Unmanned Aerial Vehicle (UAV) was also used to construct 3D photogrammetry models and DEMs of the 2016 rupture at selected locations. For each model, approximately 60 aerial photos were taken across ≥2 transects parallel to the surface rupture. Images were processed into ~2 cm/pixel DEMs and ~1 cm/pixel orthophotos using Agisoft Photoscan Professional Photogrammetry software. DJI Phantom 3 Professional onboard Global Navigation Satellite System (GNSS) was used for initial image position in photogrammetry software, and for georeferencing DEM and orthophotos. Ground control points were not used, so the horizontal accuracy of these models is based on the UAV's onboard GNSS, which is <5 m. The internal accuracy in these models (which is used is for measuring scarp height) is estimated from the size of the smallest resolvable 'real' feature, and is considered to be 5 cm.

Surface rupture observations along the Hundalee Fault

Kaikōura Earthquake surface rupture of the Hundalee Fault is comprised of a series of complex and discontinuous (<1 km) traces. These are summarized by the surface rupture maps in Fig. 3, and which in Fig. 3a are underlain by InSAR data (Hamling et al., 2017). This revealed a well-defined line of differential ground shift that coincides closely with the previously mapped fault. In the following section, we describe each of the key sites along the Hundalee Fault, starting in the southwest and moving towards the northeast.

Ferniehurst

An immediate target was to examine a previously mapped Late Quaternary scarp (Warren 1995; Rattenbury et al., 2006; Barrell and Townsend, 2012) immediately northeast of a railway bridge at

Ferniehurst (Fig. 3a). Here, an intact fence line that crosses the scarp indicates it did not exhibit any surface rupture in 2016 (Fig. S3a, available in the electronic supplement to this article). A traverse along the previously mapped fault trace for 2.5 km to the northeast also found no indication of surface rupture. At the most northeasterly point of this traverse, there is a broad (~0.7 km wide) high-level saddle with a large expanse of bare ground across the geologically inferred position of the fault (Figs. 3a and S1b). Though this terrain is ideal for revealing surface deformation, there was no surface cracking or, furthermore, no scarp that could represent a Holocene or even Late Pleistocene fault rupture.

These observations imply that the suspected scarp near Ferniehurst (Fig. S3a, available in the electronic supplement to this article), on lower, younger, terrain, is not tectonic, but is a fluvially-cut river terrace edge, the possibility of which was discussed in Barrell and Townsend (2012). Northeast from this area, the geologically-mapped position of the Hundalee Fault passes through hilly and thickly vegetated terrain, which we inspected from a helicopter and saw no conclusive surface rupture deformation.

InSAR analysis indicates that a ground shift with 1.0 ± 0.5 m of vertical displacement (Hamling et al.,2017; Hamling personal. comm., 23 Jan 2018) occurred for ~9 km southwest of our southernmost identified surface rupture near Hundalee (discussed below, Fig. 3a). The southern ~5 km of the InSAR-inferred rupture coincides with a 1 km wide poorly consolidated gravel plain containing the active bed of the Conway River (Fig. 3a). Here, helicopter reconnaissance revealed numerous discontinuous open cracks, however, they did not show any distinct linear trend. Therefore, they are most likely surficial cracks associated with liquefaction or lateral spreading, and the InSAR-indicated ground shift either represents surface rupture that the terrain prevented us from identifying, or diffuse ground flexure above a blind rupture at depth.

SH1 Hundalee

The southernmost unequivocal evidence of Kaikōura Earthquake surface rupture along the Hundalee Fault is a ~200 m northeast-trending rupture that crossed State Highway 1 (SH1) 3 km north of Hundalee, henceforth referred to as the SH1 Hundalee locality (Fig. 3a). Here, we recorded 1.7 ± 0.2 m of dextral offset and 1.0 ± 0.2 m uplift to the northwest, across the paint markings at the margin of the road (Fig. 4a, Table 1). In a paddock immediately west of SH1, the rupture was defined by sinuous left stepping *en-echelon* pressure ridges that ran at a high angle to a series of tensional fissures (Figs. 4b and c). To the northeast of SH1, the rupture could be traced as far as the margin of a landslide that was reactivated by the earthquake.

Limestone Stream

Across the floor of Limestone Stream, a 150 m long rupture with a northeasterly trend was observed (Fig. 3a). Aerial photographs indicate that there was no pre-existing scarp at this locality, so the 2016 vertical fault offset could be determined from the total scarp height, which was 2.0 ± 0.3 m to the north (Fig. S4, available in the electronic supplement to this article). No reliable markers to quantify horizontal offset were observed at this locality. A 30 m wide zone of comminuted greywacke was observed. This trace could be mapped for a further 200 m to the southwest by lidar. To the northeast, it can be inferred to extend across steep terrain for another 150 m where it adjoins a north-northeast trending rupture trace that extended for ~0.6 km across partly forested hill terrain (Fig. 3). This section was mapped from helicopter observations but not inspected on the ground.

Okarahia

Surface rupture was identified on a south bank terrace of Okarahia Stream about 3.8 km to the northeast of the SH1 Hundalee locality (Fig. 3a). The 190-m long north-trending trace exhibits 0.5 ± 0.1 m of uplift to the west (Fig. 5a), in which slabs of soil and roots were bent and buckled to form ‘turf rolls’ (e.g. Beanland et al., 1989; Little et al., 2018). Fences that cross the scarp at a high angle indicate 0.6 ± 0.15 m of sinistral offset (Fig. 5b, Table 1). There is a topographic step at the same location that is ~1 m higher than the 2016 scarp and is interpreted to be a pre-existing fault scarp (Fig. 5a). The 2016 fault scarp could not be traced along strike on high topography on either side of the Okarahia Stream valley. This site lies ~0.5 km southeast of the geologically mapped position of the Hundalee Fault (Fig. 3a).

Glenstrae

At Glenstrae farm there is a continuous 0.9 km long northeast-trending 2016 surface rupture trace. Its southwestern end lies about 0.8 km to the north of the Okarahia locality and is also within ~1.5 km of the south-southeastern limit of the Stone Jug Fault surface ruptures (Fig.3a; Stirling et al., 2017; Nicol et al., 2018). This uphill facing trace runs along a moderate to steep slope on the southwest side of the Te Kahika Stream valley, ~60 m above the stream level. The slope is extensively hummocky with several minor basins each separated by a longitudinal ridge parallel to the fall of the slope. On the ridges, the 2016 rupture coincides with a small (<50 cm) topographic step that we interpret to be a pre-existing fault scarp (Fig. S5a, available in the electronic supplement to this article). The extensive landslide terrain suggests a relatively youthful land surface and so the most recent previous rupture is probably no older than Holocene.

Overall offset was 0.9 ± 0.1 m upthrow to the northwest and as much as 0.9 ± 0.1 m sinistral (Table 1). This low degree of uncertainty was achieved by matching broken, or stretched but unbroken, tree roots where the rupture crossed a stand of trees (Fig. 6a). Furthermore, the 2016 scarp crosses several fence-lines at a high angle to the fault, and these provide displacement markers that allow a sinistral component of offset as small as 0.3 ± 0.1 m to be defined with confidence (Fig. 6b, Table 1).

The Birches

Near ‘The Birches’ homestead, on the lowest valley-floor terraces of Te Moto Moto Stream, we identified three, approximately parallel, north to northeast trending 2016 rupture traces (Fig. 3b). Between the southwestern end of these ruptures and the northeastern end of the Glenstrae ruptures, differential lidar indicates a lineament with relative uplift, however, no surface rupture was observed (Fig. 7). It is unclear whether the deformation through this area consisted of flexure or simply involved rupture that was not recognizable due to the steep and vegetated terrain.

All three traces at the Birches locality show uplift to the west or northwest (Fig. 3b, Table 1). The westernmost (Birches-1) consists of a 1.0 ± 0.2 m high scarp where a stream terrace riser and a rutted vehicle track illustrate sinistral offset of 1.2 ± 0.2 m (Fig. 8, Table 1). Approximately 200 m along strike to the north, on a high terrace, there is no visible indication of deformation of fence lines, implying that the Birches-1 trace dies out a short distance north of Te Moto Moto Stream (Fig. 3b). A ~120 m long sinuous turf roll with a 0.5 ± 0.1 m component of vertical offset, and no clear indication of lateral movement comprises the Birches-2 trace (Table 1, Fig. S6a, available in the electronic supplement to this article). The Birches-3 trace comprises a 0.9 ± 0.2 m high scarp. A road that crosses the southern end of scarp shows no strike-slip offset, however, 80 m north along the scarp we observed 0.5 ± 0.1 m sinistral offset of a stream channel edge (Table 1, Fig. S6b, available in the electronic supplement to this article).

Where the Birches-1 fault scarp crosses the Te Moto Moto Stream, a ~60 m wide sequence of fault rocks derived from the Pahau Terrane greywacke is exposed on the uplifted side of the fault (Fig. 9). Adjacent to the rupture trace, there is a ~5 m wide zone of pale grey fault breccia that contains rare lenses of intact rock of up to 30 cm across. Anastomosing fault gouges <10 cm thick and dipping approximately 60° to the NW (Fig. 9a) are contained within the breccia. Fine-grained black material also occurs in a subsidiary network of gently dipping fractures. However, it is not clear if these represent gouges derived from attrition of fault rocks or frictional-melt derived pseudotachylyte in injection veins (Fig. 9b). *En echelon* veins less than 1 cm wide are also observed within the breccia (Fig. 9d). Upstream from the fault breccia zone is highly fractured greywacke, though the original sedimentary bedding is still apparent (Fig. 9e). The intensity of fracturing progressively decreases westward, although there are still some <1 m thick intervals of fault breccia (Fig. 9f). Under conventional models of fault zone structure (e.g. Chester and Logan, 1986; Chester et al., 1993; Caine et al., 1996), the ~5 m thick sequence of gouges and breccias adjacent to the rupture trace would be considered to comprise the fault core, and the damage zone would be represented by the fractured greywacke.

Glencree

On a narrow terrace ~60 m above the north bank of Te Moto Moto Stream at Glencree farm (Fig. 3b), a 0.4 ± 0.1 m high turf roll, up to the west, passes between two houses (Table 1, Fig. S7, available in the electronic supplement to this article). This surface rupture lies roughly along trend from the Birches-3 trace. However, ~100 m farther north along trend in the Oaro River valley, there is no offset of the adjacent, low-level west bank river terraces. This constrains the tip of this rupture trace to somewhere between the Glencree terrace and the bottom of the Oaro River valley (Fig. 3b).

Oaro Left Bank

Northeast from the Oaro River to the coast is a complex array of predominantly northeast-trending 2016 surface rupture traces (Fig. 3b). Individual rupture traces range from ~40 m to ~1 km in length and show large variations in offset (Fig. 3b, Table 1). The westernmost trace (Oaro left bank-1) consists of an east-northeast scarp with a maximum height of 2.5 ± 0.5 m. This measurement is the maximum vertical displacement across a single trace of the Hundalee Fault for the Kaikōura Earthquake (Table 1). In most places deformation is distributed across a zone as much as 20 m wide (Fig. 10). An offset deer fence revealed a sinistral component of movement of 1.1 ± 0.2 m (Table 1). To the northeast, there is a discontinuous array of surface ruptures traces that show either no identifiable lateral component or a small amount of dextral offset, such as the Oaro left bank-2 trace, where a deer fence is offset 1.0 ± 0.5 m vertically and up to 0.4 ± 0.2 m dextrally. This trace and the adjacent Oaro left bank-3 trace differ from all others on the Hundalee Fault, being downthrown to the northwest (Table 1, Fig. S8, available in the electronic supplement to this article). Further along-trend, the Oaro left bank-4 trace shows reverse-dextral motion, but with the 1.0 ± 0.5 m of uplift to the northwest (Fig. 3b).

SH1 Coast

Hundalee Fault surface ruptures crossed SH1 at the coast at two localities, 400 m apart (Fig. 3b). The southernmost of these is a west-northwest trending horizontal flexure (SH1 Coast-1) with an offset of 0.4 ± 0.1 m up to the north and 0.7 ± 0.2 m dextral (Fig. 3b, Table 1). Across the highway, the 2016 rupture produced a left-stepping *en-echelon* array of diffuse fractures (Fig. S9a, available in the electronic supplement to this article). In farmland to the west, there is no ground cracking, but there was definitive flexure of fences over a ~30 m wide deformation zone (Fig. S9b, available in the electronic supplement to this article).

The largest measured horizontal offset of the Hundalee Fault 2016 ruptures is across a prominent 450 m northeastern trending trace (SH1 Coast-2), which is along trend from the Oaro left Bank-4 trace (Fig. 3b). The trend of the rupture at this locality and that of the SIMT railway and SH1 differ by only ~20º (Fig. 11a), making projection of piercing points difficult, especially as both the road and rail curve at the rupture location. By comparing pre- and post-earthquake aerial photography and matching up the painted road lines (including the marginal rumble strips), we determined an offset of 3.7 ± 0.5 m dextral and 1.5 ± 0.5 m vertical (Table 1). By applying a near-vertical fault plane to these measurements, Litchfield et al., (2018) calculated a net slip of 4.0 ± 0.7 m, which is the largest measured across the Hundalee Fault for this event. In the shore platform, the 2016 rupture and associated uplift exposed fault gouge within greywacke on the upthrown side of the fault (Fig. 11b). These localities mark the southernmost extent of coastal uplift that formed during the Kaikōura Earthquake (Clark et al., 2017). Multibeam bathymetry surveying of the seafloor identified a scarp that is continuous with our onshore mapping of the Hundalee Fault and extends for at least 2 km towards the edge of the Kaikōura canyon system (Stirling et al., 2017; Litchfield et al. 2018).

Discussion

Summary of slip distribution and kinematics along the Hundalee Fault

To provide a better understanding of Kaikōura Earthquake rupture of the Hundalee Fault, we compared all offset measurements (Table 1) to their position along strike of the fault, as mapped from bedrock relationships (Figs. 12a-b). Measurements from locations that are off the line of the mapped bedrock position of the fault (e.g. Okarahia) are projected at approximate right angles onto the fault alignment. To provide clarity, a single representative measurement for each locality is shown in Fig. 12c. Where surface ruptures have an *en-echelon* arrangement, we have also summed the offset measurements in Fig. 12c from individual strands (as shown in Fig. 3). Note, we have not aggregated the SH1 Coast offsets, because the two traces have strike approximately perpendicular to one another (Fig. 3b). Measurements derived from InSAR (Hamling et al., 2017) along the southern section of the Hundalee Fault are also included.

Fig. 12 indicates the total length of surface rupture quantified by field observations is ~12 km. However, when we also account for the rupture inferred from InSAR observations (an additional 9 km, Fig. 3a) and offshore from marine surveys (an additional 2 km; Stirling et al., 2017), the total length of Kaikōura Earthquake rupture along the Hundalee Fault is ~23 km.

By summing offsets across *en-echelon* traces, the highest vertical displacement is observed along the central part of the Hundalee Fault where >2 m of offset is noted. In this context, the <1 m vertical offset at the Okarahia and Glenstrae localities is anomalously low, which suggests that deformation may be distributed across additional traces at these localities that we could not identify (as represented by the dashed lines for vertical slip in Fig. 12c). Horizontal displacements show more scatter, with the maximum displacement recorded at the SH1 Coast-2 locality (Fig. 12c). However, no horizontal offset measurements could be made by offshore surveys, so it is unclear whether this locality represents the maximum horizontal co-seismic displacement along the Hundalee Fault, or if it increases offshore to the northeast. We also recognize that some of our measurements are within a few meters either side of the ruptures and may not have accounted for all the distributed off-fault deformation (if any) across the Hundalee Fault (Kearse et al., 2018 Dolan and Haravitch, 2014).

Analyses of rupture trace orientation and our offset measurements allow us to characterize the 2016 slip distribution as three adjoining sections (Figs. 3, 12 and 13). Oblique dextral-reverse slip along northeast trending rupture traces characterizes the south and north sections, while the central section contains north to north-northeast trending ruptures with reverse-sinistral slip (Fig. 13). At a broad scale, the co-existence of dextral-reverse slip along northern and southern strands of the Hundalee Fault and reverse-sinistral slip along central strands may be explained by contraction about a single axis with an orientation of 120 ± 10° (Fig. 13). This implies that the ratio of vertical slip to horizontal slip should be highest in the central section, as is generally observed (Fig. 12c).

The kinematics and fault trends of the Hundalee Fault are similar to those documented elsewhere for the Kaikōura Earthquake. For example, strike-slip movement is observed along east-west trending faults (e.g. The Humps Fault (west); Nicol et al., 2018), dextral-reverse motion along northeast trending faults (e.g. Conway-Charwell Fault; Nicol et al., 2018) and reverse-sinistral movement along north to north-northeast trending faults (e.g. Leader and Papatea Faults; Nicol et al., 2018; Langridge et al., 2018). Furthermore, the contraction axis our observations indicate (120 ± 10°) is similar to the regional principal axis of horizontal contraction derived from geodetic studies (116 ± 9°; Pearson et al., 1995), and the azimuth of the regional principal compressive stress (σ_1) reported from seismology (115 ± 16°; Balfour et al., 2005; Townend et al., 2012) and structural analysis (122 ± 17°; Nicol and Wise, 1992; 114 ± 9°; Sibson et al., 2012).

Sinistral displacement along the ENE trending Oaro Left Bank-1 locality (Figs. 3 and 13) is not, however, consistent with this contraction azimuth. This localized kinematic anomaly may reflect its position between the transfer of displacement between central and northern sections. The Oaro Left Bank-2 and 3 localities also show uplift to the south and southeast, which is inconsistent with the

2016 upthrow reported elsewhere along the Hundalee Fault, and with the net Late Cenozoic throw that has elevated greywacke ranges to the northwest of the fault. One possibility is that they could attest to the existence of an otherwise ill-defined local transtensional jog on the northern section of the Hundalee Fault.

Variability of expression in the 2016 rupture

Much of the terrain along the Hundalee Fault is relatively young, comprising eroding hill slopes and river or stream valley floors. Therefore, one of the challenges in mapping the 2016 surface rupture was in distinguishing superficial slope-related movement from true tectonic displacement. Fortuitously, where uncertainties might be raised about gravitational influences on some observed Hundalee Fault surface rupture offset (e.g. Oaro Left Bank-2 and -3), there are many clear examples of displacements across areas with low to moderate slopes such as floodplains, low river terraces and gently rolling hill country. We are therefore confident that our Hundalee Fault surface rupture observations reflect tectonic motions.

Quaternary-age sediments form only a thin veneer over cover strata or greywacke around the Hundalee Fault (e.g. the Oaro Left Bank-1 site, Fig. 10). This is largely due to long-term regional uplift that is documented by flights of uplifted marine terraces along the coast (Warren 1995; Rattenbury et al., 2006). This combination of thin Quaternary deposits and the relatively youthful terrain entails that many sites may not have recorded earlier Hundalee Fault events. Exceptions to this are at the Okarahia (Fig. 7) and Glenstrae localities (Fig. 8), and on some slopes near the coast that may be suitable for future paleoseismic investigations.

Kaikōura Earthquake surface ruptures vs. longer term behavior of the Hundalee Fault

Rupture along the Hundalee Fault during the Kaikōura Earthquake produced highly irregular and discontinuous surface ruptures (Fig. 3). As a way of comparing the 'complexity' of the Hundalee Fault rupture to global compilations, we calculated its total absolute angular deflection (TAAD; Biasi and Wesnousky, 2017). This is the sum of all angular deflections interior to mapped rupture traces, with the requirement that each rupture segment is >5-7 km in length. To apply this to the Hundalee Fault, we therefore only measure the angles between its inferred southern, central and northern sections (Fig, 13). This gives a TAAD of 98°, which when normalized to rupture length (i.e. 23 km) is 4.3 °/km (2 significant figures). By comparison, Biasi and Wesnousky (2017) report median curvature values of TAAD for strike-slip and dip-slip ruptures of 0.5 and 1.6°/km respectively from their compilation of 67 historical ruptures. Therefore, the 2016 rupture of the Hundalee Fault was complex using the criterion of Biasi and Wesnousky (2017).

A high degree of rupture complexity and distributed deformation along the Hundalee Fault could be explained by either: (1) thick deposits of poorly consolidated sediments (Zinke et al., 2015), (2) the surrounding topography (Khajavi et al., 2014), (3) its orientation with respect to bedding (Heermance et al., 2003), or (4) that it is 'structurally immature' (Perrin et al., 2016). As noted above, only thin deposits of Quaternary-age sediments are found around the Hundalee Fault, and so the first point is unlikely to have contributed to surface rupture complexity. However, it is conceivably that rupture complexity may have been imparted by the along-strike changes in topography across the Hundalee Fault (Fig. 13), and the fact that it trends at a high angle to the bedding of the Torlesse greywacke (Rattenbury et al., 2006).

The implication that the Hundalee Fault is structurally immature, is that it has not accumulated sufficient displacement for slip to become focused into a continuous mechanically efficient planar zone (Wesnousky, 1988; Stirling et al., 1996; Manighetti et al., 2007; Finzi et al., 2009; Cooke and Madden, 2014; Zinke et al., 2015). This is important as the cumulative effect of structural maturation is a large disparity in the type of earthquakes along immature and mature faults in terms of stress drops (Anderson et al., 1996), ground motions (Radiguet et al., 2009), and rupture extents and propagation velocities (Wesnousky, 2006; Manighetti et al., 2007; Perrin et al., 2016). To the first order, this principle is consistent with the other faults that ruptured during the Kaikōura Earthquake.

Structurally immature faults in the NCD (e.g. The Humps Fault, Leader Fault zone; Fig. 1) tended to rupture in discontinuous strands (Litchfield et al., 2018; Nicol et al., 2018), whereas the faster slipping more established faults in the MFS (e.g. Kekerengu Fault, Needles Fault; Fig. 1) exhibited more continuous rupture traces (Kearse et al., 2018; Litchfield et al., 2018).

Nevertheless, though the discontinuous non-planar ruptures that we document along the Hundalee Fault are suggestive of a structurally immature fault, it has clearly accommodated a significant amount (>1 km) of Late Cenozoic throw (see Geological Setting section). Furthermore, it is associated with a thick (<60 m) section of fault rocks at the Birches-1 site that include narrow (<10 cm thick) gouge zones (Fig. 9a). These indicate that the Hundalee Fault has, at least in the past, localized slip into very narrow zones as would be anticipated for structurally mature faults (Heermance et al., 2003; Sibson, 2003; Rockwell and Ben-Zion, 2007). Though we cannot be certain that this section is representative of the entire length of the Hundalee Fault, some along-strike continuity is provided by the <10 cm thick gouge zones ~5 km to the northeast at the SH1-Coast-2 locality (Fig. 11b), and 7 km to the southwest at Limestone Stream.

To resolve the apparent paradox between our observation of complex Hundalee Fault surface rupture, and its structural maturity implied by geological mapping and its fault rocks, we consider it pertinent that it represents just one fault of possibly 20 that ruptured during the Kaikōura Earthquake. A 3D structural model of those faults that ruptured in the NCD suggests that they may share some sort of physical connection at depth (Hamling et al., 2017; Litchfield et al., 2018). Therefore, the efficiency with which the Kaikōura Earthquake rupture propagated across these connections would reflect the structural maturation of this larger Humps-Leader- Conway Charwell-Stone Jug-Hundalee multi-fault system (Fig. 1; Cooke and Kameda, 2002; Griffith and Cooke, 2004), and not necessarily the maturity of each individual fault.

Important questions, however, remain regarding the subsurface geometry of the NCD faults that ruptured in 2016. Although the NCD 3D fault model implies that the fault dip measured at the surface persists throughout the seismogenic zone (Litchfield et al., 2018) this is not necessarily the case (e.g. Heermance et al., 2003; Li et al., 2013). Indeed, it is possible that the Hundalee Fault is listric at depth and is linked with other similarly oriented faults along a low-angle detachment. Such a scenario has been proposed for faults further south in the NCD, which have been interpreted to be linked by a detachment at depth of ~12 km (Nicol et al., 2018; Reyners and Cowan, 1993; Campbell et al., 2012; Litchfield et al., 2014a). Constraining the hitherto poorly-constrained subsurface geometry and connectivity of the NCD faults (e.g. through active-source geophysical techniques, aftershock distribution analysis) is important, as this will illuminate: (1) the tendency of earthquake ruptures to propagate across multiple faults in this network (Biasi and Wesnousky, 2016, 2017; Fletcher et al., 2016), and (2) the efficiency with which they do so (Cooke and Kameda, 2002).

Conclusions

The 2016 M_W 7.8 Kaikōura Earthquake ruptured the northeastern section of the Hundalee Fault. Field observations indicate rupture over a length of ~12 km, with an additional ~9 km of surface deformation extending southwest indicated by InSAR (Fig. 3; Hamling et al., 2017) and 2 km of rupture offshore indicated by marine surveys (Stirling et al., 2017). Surface rupture was typically oblique with dextral-reverse motion along northeast trending sections in the southern and northern ruptures of the Hundalee Fault, and reverse-sinistral motion along north and north-northeast trending sections along the central section of the fault. This can be explained by contraction along an axis of 120 ± 10º, consistent with other faults that ruptured in the Kaikōura Earthquake (Nicol et al., 2018) and with regional plate motions (Pearson et al., 1995). The amount of slip varied along strike of the Hundalee fault (Fig. 12), with a maximum vertical offset of 2.5 ± 0.5 m and maximum strike-slip offset of 3.7 ± 0.5 m.

The 2016 Hundalee Fault rupture was characterized by discontinuous strands that deformed the ground in a range of styles from sharp scarps to ground warping across a zone tens of meters wide. This rupture style is suggestive of an immature fault, yet previous mapping and evidence of localized slip within a thick fault-rock sequence indicate that the Hundalee Fault is a mature fault. This discrepancy is one of many unanticipated outcomes of the complex Kaikōura Earthquake.

Data and Resources

All data used in this paper is original except when cited from the published sources listed in the references. Map in Figs. 3 and 13 generated using QGIS (http://www.qgis.org/en/site/). The underlay of these figures was obtained from the New Zealand 8 m Digital Elevation Model (https://data.linz.govt.nz/layer/51768-nz-8m-digital-elevation-model-2012/).

Acknowledgements

We thank the many landowners who allowed us access to the Hundalee Fault ruptures during the 2016 November and December fieldwork. We are grateful to Barry McDowell (Tonkin and Taylor Ltd) for alerting us to the existence of the surface rupture at Okarahia. Luke Easterbrook-Clarke is thanked for constructing the UAV derived orthophoto (Fig. 4c) and DEM (Fig. 10b and c). We also thank Narges Khajavi and Andy Nicol for useful discussions in relation to the fault mapping. Ian Hamling kindly provided the InSAR data used in Fig. 3a. Photo credits; Figs. 4a and b, 6, 8, 10a, 11b, S3, S4, S5, S6b, S7, S9– DJA Barrell, GNS Science; Fig. 5 – KM Sauer; Figs. 9, S6a – JN Williams; Fig. S8 – MW Stirling; Fig. 11a - NZ Transport Agency. This manuscript was improved by thoughtful and constructive reviews by Christopher DuRoss, an anonymous reviewer, and comments by its handling editor, Timothy Stahl.

References

Anderson, J., S.G. Wesnousky, and M.W. Stirling (1996). Earthquake size as a function of fault slip rate, *Bull. Geol. Soc. Am*. **86** 683–690.

Balfour N.J., M.K. Savage and J. Townend (2005). Stress and crustal anisotropy in Marlborough, New Zealand: Evidence for low fault strength and structure-controlled anisotropy, *Geophys. J. Int*. **163(3), 1073-1086**

Barrell, D.J.A. (2015). General distribution and characteristics of active faults and folds in the Kaikoura District, North Canterbury. *GNS Science Consultancy Report 2014/210; Environment Canterbury Report R15/23. Christchurch, New Zealand; Environment Canterbury Regional Council.*

Barrell, D.J.A., and D.B. Townsend (2012). General distribution and characteristics of active faults and folds in the Hurunui District, North Canterbury. *GNS Science Consultancy Report 2012/113; Environment Canterbury Report R12/39. Christchurch, New Zealand; Environment Canterbury Regional Council.*

Beanland, S., K. Berryman and I. Nairn (1989). Geological setting of the 1987 Edgecumbe earthquake, New Zealand. *New Zeal. J. Geol. Geophys.* **32(1)**, 73-91.

Biasi, G.P., and S.G. Wesnousky, S. G. (2017). Bends and Ends of Surface Ruptures. *Bull. Seismol. Soc. Am.*, **107(6)**, 2543-2560.

Biasi, G.P., and S.G. Wesnousky, S. G. (2016). Steps and gaps in ground ruptures: Empirical bounds on rupture propagation. *Bull. Seismol. Soc. Am.*, **106(3),** 1110-1124.

Caine, J.S., J.P. Evans, and C.B. Forster (1996). Fault zone architecture and permeability structure, *Geology* **24,** 1025–1028.

Campbell, J.K., J.R. Pettinga, and R. Jongens (2012). The tectonic and structural setting of the 4 September 2010 Darfield (Canterbury) earthquake sequence, New Zealand. *New Zeal. J. Geol. Geophys.* **55(3)**, 155-168.

Clark, K., E. Nissen, J. Howarth, I. Hamling, J. Mountjoy, W. Ries, K. Jones, S. Goldstein, U. Cochran, P. Villamor, S. Hreinsdóttir, N. Litchfield, K. Berryman, and D. Strong (2017). Highly variable coastal deformation in the 2016 MW7.8 Kaikōura earthquake reflects rupture complexity along a transpressional plate boundary, *Earth Planet. Sci. Lett.* **474**, 334-344.

Chester, F.M., J.P. Evans, and R.L. Biegel (1993). Internal structure and weakening mechanisms of the San Andreas Fault, *J. Geophys. Res*. **98** 771-786. doi:10.1029/92JB01866

Chester, F.M., and J.M. Logan (1986). Implications for mechanical properties of brittle faults from observations of the Punchbowl fault zone, California, *Pure Appl. Geophys*. PAGEOPH **124** 79–106. doi:10.1007/BF00875720

Cooke, M.L., and E. H. Madden (2014). Is the Earth lazy? A review of work minimization in fault evolution, *J. Struct. Geol.* **66**, 334–346. doi:10.1016/j.jsg.2014.05.004

Cooke, M.L., and A. Kameda (2002). Mechanical fault interaction within the Los Angeles Basin: A two-dimensional analysis using mechanical efficiency. *J. Geophys. Res. Solid Earth* **107(B7)**.

Dolan, J.F., and B.D Haravitch, (2014). How well do surface slip measurements track slip at depth in large strike-slip earthquakes? The importance of fault structural maturity in controlling on-fault slip versus off-fault surface deformation. *Earth and Planetary Sci. Lett.* **388**, 38-47.

Finzi, Y., E.H. Hearn, Y. Ben-Zion, and V. Lyakhovsky (2009). Structural properties and deformation patterns of evolving strike-slip faults: Numerical simulations incorporating damage rheology. *Pure Appl. Geophys*. **166**, 1537–1573. doi:10.1007/s00024-009-0522-1

Fletcher, J.M., M.E. Oskin, and O.J. Teran (2016). The role of a keystone fault in triggering the complex El Mayor-Cucapah earthquake rupture. *Nat. Geosci* **9**, 303–307. doi:10.1038/NGEO2660

Griffith, W. A., and M. L. Cooke (2004). Mechanical validation of the three-dimensional intersection geometry between the Puente Hills blind-thrust system and the Whittier fault, Los Angeles, California. *Bull. Seismol. Soc. Am.* **94(2)**, 493-505.

Hamling, I.J., S. Hreinsdóttir, K. Clark, J. Elliott, C. Liang, E. Fielding, N. Litchfield, P. Villamor, L. Wallace, T.J. Wright, E. D'Anastasio, S. Bannister, D. Burbidge, P. Denys, P. Gentle, J. Howarth, C. Mueller, N. Palmer, C. Pearson, W. Power, P. Barnes, D.J.A. Barrell, R. Van Dissen, R. Langridge, T. Little, A. Nicol, J. Pettinga, J. Rowland, and M. Stirling (2017). Complex multifault rupture during the 2016 M w 7.8 Kaikōura earthquake, New Zealand. *Science*. **356**, 6334, eaam7194. doi:10.1126/science.aam7194

Heermance, R., Z.K. Shipton, and J.P. Evans (2003). Fault structure control on fault slip and ground motion during the 1999 rupture of the Chelungpu fault, Taiwan. *Bull. Seismol. Soc. Am*. **93**, 1034–1050. doi:10.1785/0120010230

Heron, D., (2014). Geological map of New Zealand 1:250,000 - digital data. *GNS Science geological map 1. 1 CD. Lower Hutt, New Zealand; GNS Science.*

Kaiser, A., N. Balfour, B. Fry, C. Holden, N. Litchfield, M. Gerstenberger, E. D'Anastasio, N. Horspool, G. McVerry, J. Ristau, S. Bannister, A. Christophersen, K. Clark, W. Power, D. Rhoades, C. Massey, I. Hamling, L. Wallace, J. Mountjoy, Y. Kaneko, R. Benites, C. Van Houtte, S. Dellow, L. Wotherspoon, K. Elwood, and K. Gledhill (2017). The 2016 Kaikōura, New Zealand, Earthquake: preliminary seismological report, *Seismol. Res. Lett.* **88**, 727–739. doi:10.1785/0220170018.

Kearse, J., T.A. Little, R.J. Van Dissen, P.M. Barnes, R.M. Langridge, J. Mountjoy, W.F. Ries, P. Villamor, K.J. Clark, A. Benson, G. Lamarche, M. Hill, and M. Hemphill-Haley (2018). Onshore to Offshore Ground-Surface and Seabed Rupture of the Jordan–Kekerengu–Needles Fault Network during the 2016 Mw 7.8 Kaikoura Earthquake, New Zealand, *Bull. Seismol. Soc. Am.* doi:10.1785/0120170304 (this issue).

Khajavi, N., M. Quigley, and R. Langridge (2014). Influence of topography and basement depth on surface rupture morphology revealed from LiDAR and field mapping, Hope Fault, New Zealand, *Tectonophysics,* **630,** 265-284

Langridge, R.M., Ries, W.F., Litchfield, N.J., Villamor, P., Van Dissen, R.J., Barrell, D.J.A., Rattenbury, M.S., D.W. Heron, S. Haubrock, D.B. Townsend, J.M. Lee, K.R. Berryman, A. Nicol, S.C. Cox, and M.W. Stirling (2016). The New Zealand active faults database, *New Zeal. J. Geol. Geophys.* **59**, 86–96. doi:10.1080/00288306.2015.1112818

Langridge, R.M., J. Rowland, P. Villamor, J.J. Mountjoy, C. Madugo, D.B. Townsend, A. Cavana, K.J. Clark, R.V. Dissen, W.R. Ries, C. Gasston, B. Hall, A. Hatem, and I. Hamling (2018). Geology, co-seismic rupture and slip on the Papatea fault and its role in the 2016 Kaikōura Earthquake, New Zealand, *Bull. Seismol. Soc. Am*. (this issue).

Li, H., H. Wang, Z. Xu, J. Si, J. Pei, T. Li, Y. Huang, S.R. Song, L.W. Kuo, Z. Sun, M.L. Chevalier, and D. Liu (2013). Characteristics of the fault-related rocks, fault zones and the principal slip zone in the Wenchuan Earthquake Fault Scientific Drilling Project Hole-1 (WFSD-1), *Tectonophysics* **584**, 23–42. doi:10.1016/j.tecto.2012.08.021

Litchfield, N., R. Van Dissen, R. Sutherland, P. Barnes, S. Cox, R. Norris, R.J. Beavan, R. Langridge, P. Villamor, K. Berryman, M. Stirling, A. Nicol, S. Nodder, G. Lamarche, D. Barrell, J.

Pettinga, T. Little, N. Pondard, J. Mountjoy, and K. Clark (2014a). A model of active faulting in New Zealand, *New Zeal. J. Geol. Geophys*. **57**, 32–56. doi:10.1080/00288306.2013.854256

Litchfield, N.J., R. Van Dissen, S. Hornblow, M. Quigley, and G. Archibald (2014b). Detailed analysis of Greendale Fault ground surface rupture displacements and geometries, *GNS Science Report* 2013/18. 166 p.

Litchfield, N.J., P. Villamor, R. Van Dissen, A. Nicol, P.M. Barnes, D.J.A. Barrell, J.R. Pettinga, R.M. Langridge, T.A. Little, J. Mountjoy, W.F. Ries, J. Rowland, C. Fenton, M.W. Stirling, J. Kearse, K.R. Berryman, U.A. Cochran, M. Hemphill-Haley, N. Khajavi, K. Jones, G. Archibald, C. Asher, A. Benson, K.J. Clark, S.C. Cox, C. Gasston, D. Hale, B. Hall, A. Hatem, D.W. Heron, J. Howarth, T. Kane, G. Lamarche, S. Lawson, B. Lukovic, C. Madugo, J. Manousakis, D. Noble, K. Pedley, K. Sauer, T. Stahl, D.T. Strong, D.B. Townsend, V. Toy, J. Williams, S. Woelz, and R. Zinke (2018). Surface rupture of multiple crustal faults in the Mw 7.8 2016 Kaikōura Earthquake, New Zealand *Bull. Seismol. Soc. Am.* (this issue).

Little, T.A., R. Van Dissen, J. Kearse, K. Norton, A. Benson, and N. Wang (2018). Kekerengu fault, New Zealand: timing and size of Late Holocene surface ruptures, *Bull. Seismol. Soc. Am.* doi:10.1785/0120170152 (this issue).

Manighetti, I., M. Campillo, S. Bouley, and F. Cotton (2007). Earthquake scaling, fault segmentation, and structural maturity, *Earth Planet. Sci. Lett*. **253**, 429–438. doi:10.1016/j.epsl.2006.11.004

Nicol, A., N. Khjavi, J.R. Pettinga, C. Fenton, T. Stahl, S. Bannister, K. Pedley, N. Hyland-Brook T. Bushell, I. Hamling, J. Ristau, D. Noble[1], and S. T. McColl (2018). Preliminary geometry, slip and kinematics of fault ruptures during the 2016 M_W 7.8 Kaikōura Earthquake in the North Canterbury region of New Zealand, *Bull. Seismol. Soc. Am.* (this issue).

Nicol, A., and D.U. Wise (1992). Paleostress adjacent to the Alpine Fault of New Zealand: fault, vein and stylolite data from the Doctors Dome area*.* *J. Geophys. Res*. **97,** 17,685-17,692.

Pearson, C.F., J. Beavan, D.J. Darby, G.H. Blick, and R.I. Walcott (1995). Strain distribution across the Australian-Pacific plate boundary in the central South Island, New Zealand, from 1992 GPS and earlier terrestrial observations. *J. Geophys. Res. Solid Earth,* **100(B11)**, 22071-22081.

Perrin, C., I. Manighetti, J.P. Ampuero, F. Cappa, and Y. Gaudemer (2016). Location of largest earthquake slip and fast rupture controlled by along-strike change in fault structural maturity due to fault growth, *J. Geophys. Res. Solid Earth* **121**, 3666–3685. doi:10.1002/2015JB012671

Pettinga, J.R., M.D. Yetton, R.J. Van Dissen, and G. Downes (2001). Earthquake source identification and characterisation for the Canterbury region, South Island, New Zealand*, Bull. New Zeal. Soc. Earthq. Eng*. **34**, 282–317.

Radiguet, M., F. Cotton, I. Manighetti, M. Campillo, and J. Douglas (2009). Dependency of near-field ground motions on the structural maturity of the ruptured faults, *Bull. Seismol. Soc. Am*. **99**, 2572–2581. doi:10.1785/0120080340

Rattenbury, M.S., D.B. Townsend, and M.R Johnston (2006). Geology of the Kaikoura area, *Inst. Geol. Nucl. Sci. 1250,000 Geol. Map. Map (1 sheet) + 70 pp. Low. Hutt, New Zealand; GNS Science*

Reyners, M., and H. Cowan, (1993). The transition from subduction to continental collision: crustal structure in the North Canterbury region, New Zealand. *Geophys. J. Int*. **115(3)**, 1124-1136.

Rockwell, T.K. and Y. Ben-Zion (2007). High localization of primary slip zones in large earthquakes from paleoseismic trenches: Observations and implications for earthquake physics. *J. Geophys. Res*. *Solid Earth*, **112(B10)**.

Sibson, R.H. (2003). Thickness of the seismic slip zone. *Bull. Seismol. Soc. Am***, 93(3)**, 1169-1178.

Sibson, R.H., F. Ghisetti, and R. A. Crookbain (2012). Andersonian wrench faulting in a regional stress field during the 2010–2011 Canterbury, New Zealand, earthquake sequenc. *Geol. Soc. London, Spec. Publ, **367(1)***, 7-18

Stirling, M., G. McVerry, M. Gerstenberger, N. Litchfield, R. Van Dissen, K. Berryman, P. Barnes, L. Wallace, P. Villamor, R. Langridge, G. Lamarche, S. Nodder, M. Reyners, B. Bradley, D. Rhoades, W. Smith, A. Nicol, J. Pettinga, K. Clark, and K. Jacobs (2012). National seismic hazard model for New Zealand: 2010 update, *Bull. Seismol. Soc. Am*. **102**, 1514–1542. doi:10.1785/0120110170

Stirling, M.W., N.J. Litchfield, P. Villamor, R.J. Van Dissen, A. Nicol, J. Pettinga, P. Barnes, R.M. Langridge, T. Little, D.J.A. Barrell, J. Mountjoy, W.F. Ries, J. Rowland, C. Fenton, I. Hamling, C. Asher, A. Barrier, A. Benson, A. Bischoff, J. Borella, R. Carne, U.A. Cochran, M. Cockroft, S.C. Cox, G. Duke, F. Fenton, C. Gasston, C. Grimshaw, D. Hale, B. Hall, K.X. Hao, A. Hatem, M. Hemphill-Haley, D.W. Heron, J. Howarth, Z. Juniper, T. Kane, J. Kearse, N. Khajavi, G. Lamarche, S. Lawson, B. Lukovic, C. Madugo, J. Manousakis, S. McColl, D. Noble, K. Pedley, K. Sauer, T. Stah, D.T. Strong, D.B. Townsend, V. Toy, M. Villeneuve, A. Wandres, J. Williams, S. Woelz, and R. Zinke (2017). The Mw7.8 2016 Kaikōura earthquake: Surface fault rupture and seismic hazard context, *Bull. New Zeal. Soc. Earthq. Eng*. **50,** 73–84.

Stirling, M.W., S.G. Wesnousky, and K. Shimazaki (1996). Fault trace complexity, cumulative slip, and the shape of the magnitude-frequency distribution for strike-slip faults: a global survey, *Geophys. J. Int.* **124,** 833–868. doi:10.1111/j.1365-246X.1996.tb05641.x

Wallace, L. M., P. Barnes, J. Beavan, R. Van Dissen, N. Litchfield, J. Mountjoy, R. Langridge, G. Lamarche, and N. Pondard (2012.) The kinematics of a transition from subduction to strike-slip: An example from the central New Zealand plate boundary, *J. Geophys. Res. Solid Earth,* **117 B2**

Warren, G., (1995). Geology of the Parnassus area: Sheets O32 & part N32, Scale 1: 50000, *Institute of Geological and Nuclear Sciences Geological Map 18. Map (1 sheet) + 36 pp. Lower Hutt, New Zealand; GNS Science.*

Wesnousky, S.G., (2006). Predicting the endpoints of earthquake ruptures, *Nature* **444**, 358–360. doi:10.1038/nature05275

Wesnousky, S.G., (1988). Seismological and structural evolution of strike-slip faults, *Nature.* 335, 340-343, doi:10.1038/335340a0

Zinke, R., J.F. Dolan, R. Van Dissen, J.R. Grenader, E.J. Rhodes, C.P. McGuire, R.M. Langridge, A. Nicol, and A.E. Hatem (2015). Evolution and progressive geomorphic manifestation of surface faulting: A comparison of the Wairau and Awatere faults, South Island, New Zealand, *Geology* **43**, 1019–1022. doi:10.1130/G37065.1

Zinke, R., J. Hollingsworth, and J.F., Dolan (2014). Surface slip and off-fault deformation patterns in the 2013 MW 7.7 Balochistan, Pakistan earthquake: Implications for controls on the distribution of near-surface coseismic slip, *Geochemistry, Geophys. Geosystems* **15**, 5034–5050. doi:10.1002/2014GC005538

Authors addresses

JW*, MS, KS and GD: Otago Earthquake Science Group, Department of Geology, University of Otago, PO Box 56, Dunedin, 9054, New Zealand

DB: GNS Science, Private Bag 1930, Dunedin, 9016, New Zealand

KXH: National Research Institute for Earth Science and Disaster Prevention (NIED), Tsukuba, Japan.

*JW now at School of Earth and Ocean Sciences, Cardiff University, Cardiff, United Kingdom, CF10 3AT

List of Tables

Table 1: Offset measurements for the Hundalee Fault 2016 rupture*

Locality	**Latitude (S)**	**Longitude (E)**	**Vertical (m). Azimuthal octant of upthrown side in parentheses**	**Horizontal (m). Shear sense in parentheses**	**Offset feature**	**Offset measurem technique**
SH1 Hundalee	42.571760	173.429079	1.0 ± 0.2 (NW)	1.7 ± 0.2 (D)	White line along NW edge of SH1 highway	RTK
Limestone Stream	42.56599	173.42723	2.0 ± 0.3 (N)		Scarp height	MT, lidar
Okarahia	42.543785	173.460041	0.5 ± 0.1 (W)	0.6 ± 0.15 (S)	Stream bed	MT
Glenstrae	42.536624	173.462583	0.3 ± 0.1 (W)	0.3 ± 0.1 (S)	Deer fence	MT
Glenstrae	42.535129	173.464751	0.8 ± 0.2 (W)	0.2 ± 0.1 (S)	Deer fence	MT

Glenstrae	42.533610	173.466348	0.8 ± 0.2 (W)	0.8 ± 0.2 (S)	Matching offset turf blocks	MT
Glenstrae	42.533275	173.466601	0.9 ± 0.1 (W)	0.9 ± 0.1 (S)	Exposed broken tree roots	MT
Birches-1	42.526496	173.468243	1.1 ± 0.2 (W)	1.1 ± 0.2 (S)	Gravel track and scarp height	MT, Lidar
Birches-1	42.526091	173.468252	1.0 ± 0.2 (W)	1.2 ± 0.2 (S)	Deer fence	MT
Birches-2	42.525620	173.473435	0.5 ± 0.1 (NW)		Scarp height	MT
Birches-3	42.524746	173.475632	1 ± 0.1 (NW)		Gravel track	MT
Birches-3	42.523835	173.475844	0.9 ± 0.2 (W)	0.5 ± 0.1 (S)	Stream bed	MT
Glencree	42.522424	173.477416	0.4 ± 0.1 (W)		Scarp height	MT
Oaro left bank-1	42.518639	173.473711	<2.2 (N)		Stream bed	Lidar, MT
Oaro left bank-1	42.518556	173.474039	2.0 ± 0.5 (N)		Scarp height	Lidar, MT
Oaro left bank-1	42.518492	173.474294		1.1 ± 0.2 (S)	Deer fence	Lidar, RTK

Oaro left bank-1	42.518237	173.474974	2.25 ± 0.25 (N)		Scarp height	Lidar, MT, UAV
Oaro left bank-1	42.518128	173.475387	2.5 ± 0.5 (N)		Scarp height	Lidar, MT
Oaro left bank-2	42.518269	173.490874	1.0 ± 0.2 (SE)	0.4 ± 0.1 (D)	Deer fence	RTK
Oaro left bank-2	42.516962	173.493408	1.0 ± 0.5 (SE)	0.08 ± 0.02 (D)	Deer fence	MT
Oaro left bank-3	42.514445	173.490113	0.8 ± 0.2 (SE)		Farm track	MT
Oaro left bank-3	42.511968	173.494379	0.4 ± 0.2 (SW)		Farm track, fence	MT
Oaro left bank-3	42.510711	173.497716	1.0 ± 0.3 (S)	0.5 ± 0.2 (D)	Farm track	MT
Oaro left bank-4	42.510022	173.496700	1.0 ± 0.3 (N)	1.5 ± 0.5 (D)	Farm track	MT
Oaro left bank-4	42.507574	173.502609	0.7 ± 0.3 (N)		Fence	MT
SH1 Coast-1	42.507634	173.507247	0.4 ± 0.1 (N)	0.7 ± 0.2 (D)	Fence	MT

SH1 Coast-2	42.504930	173.509915	1.5 ± 0.5 (N)	3.7 ± 0.5 (D)	SH1 highway	RTK

*All measurements gathered along the Hundalee Fault during field work in November and December 2016. D denotes dextral and S sinistral strike-slip offset respectively. Locations for all sites given in Fig. 3. MT, measuring tape; RTK, Real Time Kinetic global positioning system (GPS) survey; SH1, State Highway 1.

List of Figures

Figure 1

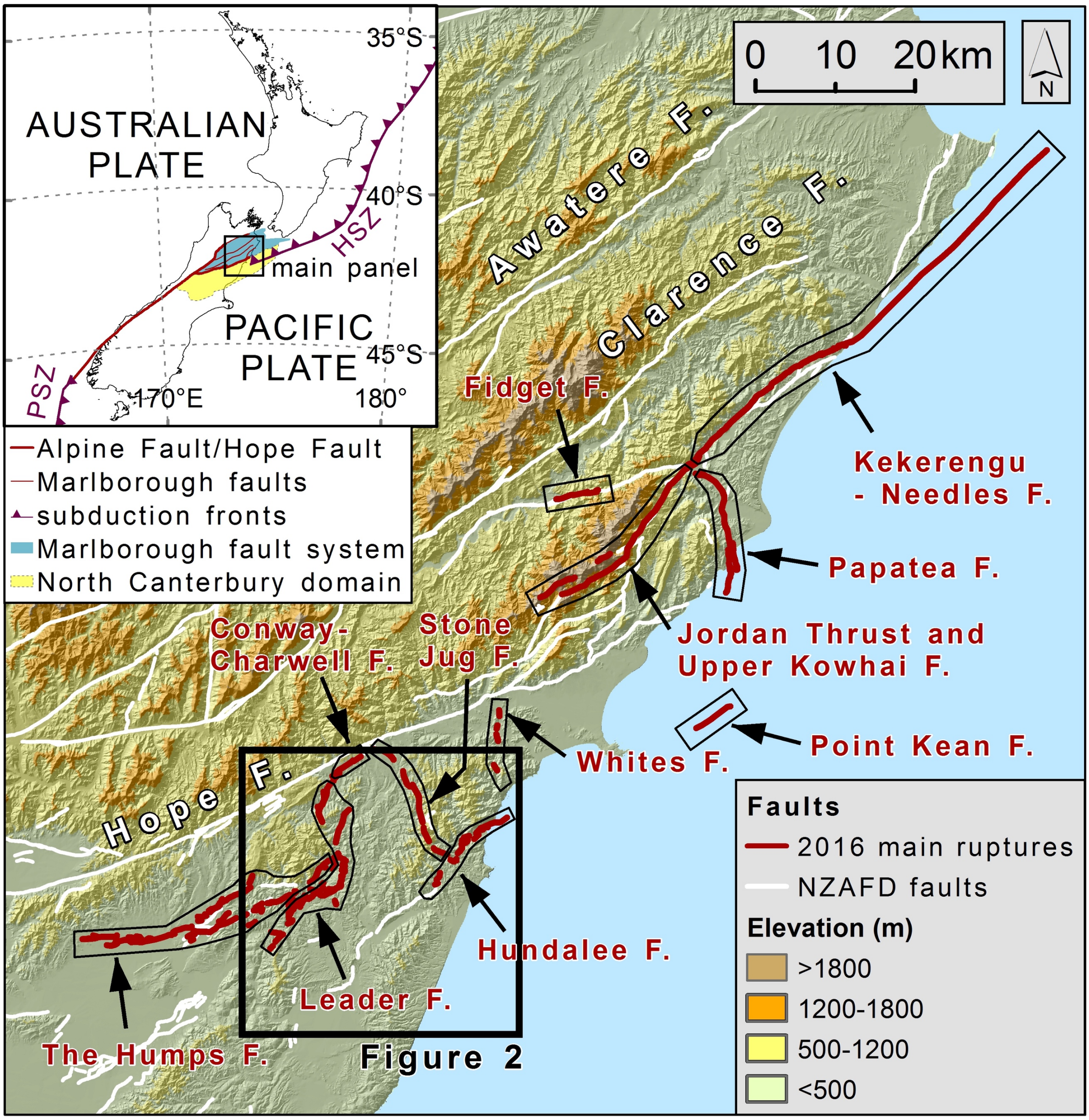

Figure 1: Map of the surface ruptures produced by the M_W7.8 2016 Kaikōura earthquake, with previously identified active faults also shown (Langridge et al., 2016). NZAFD; New Zealand active fault database. Inset depicts extent of main panel in terms of the Australian-Pacific plate boundary running through New Zealand, and the location of the North Canterbury and Marlborough Fault System tectonic domains. HSZ, Hikurangi Subduction Zone.

Figure 2

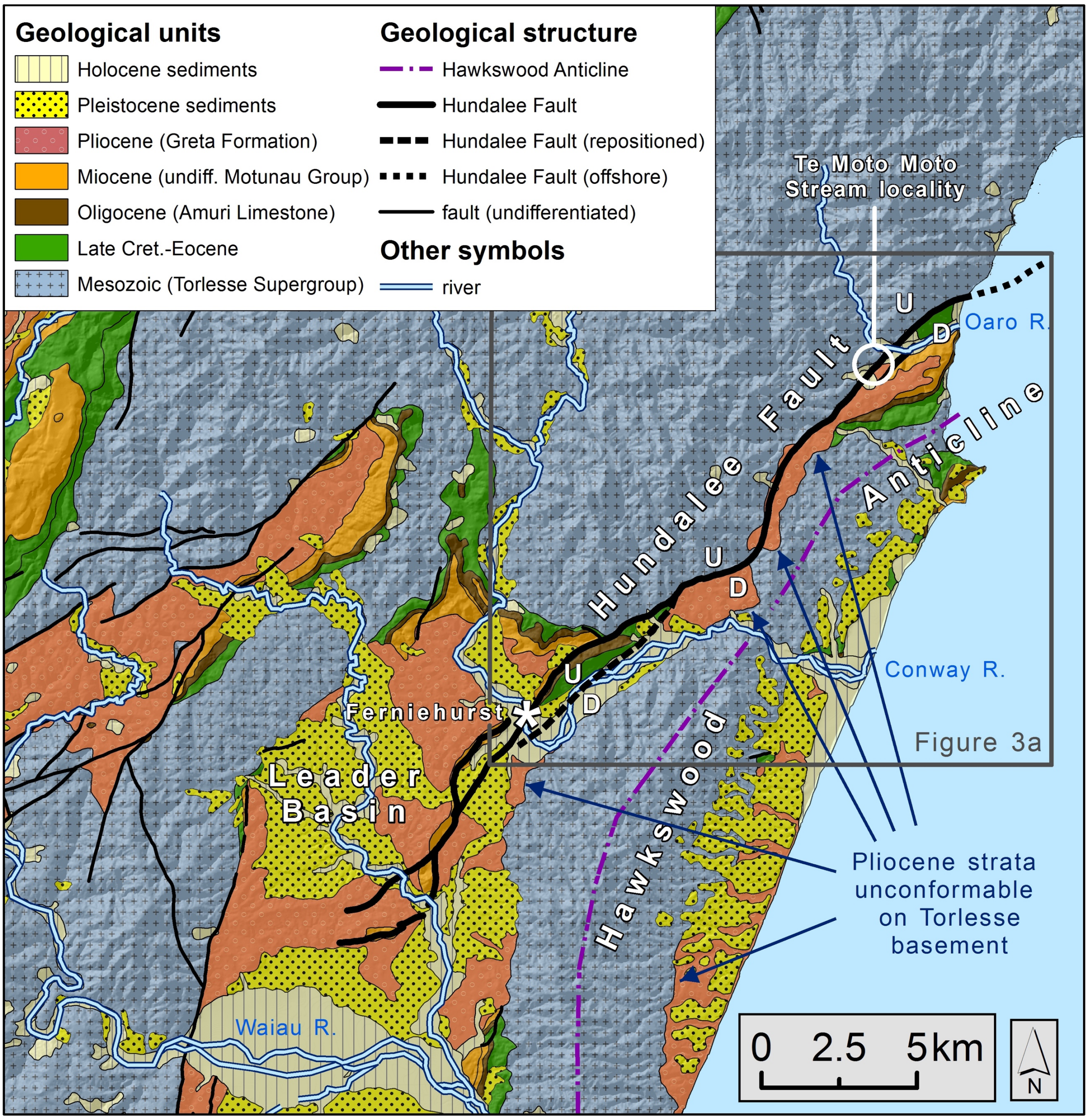

Figure 2: Geological map of the Hundalee Fault area. Derived from the QMAP 1:250,000-scale geological map database (Rattenbury et al., 2006; Heron, 2014) and underlain by a digital elevation model. A revised position for part of the Hundalee Fault (dashed black line), and additional fold axes are also shown.

Figure 3

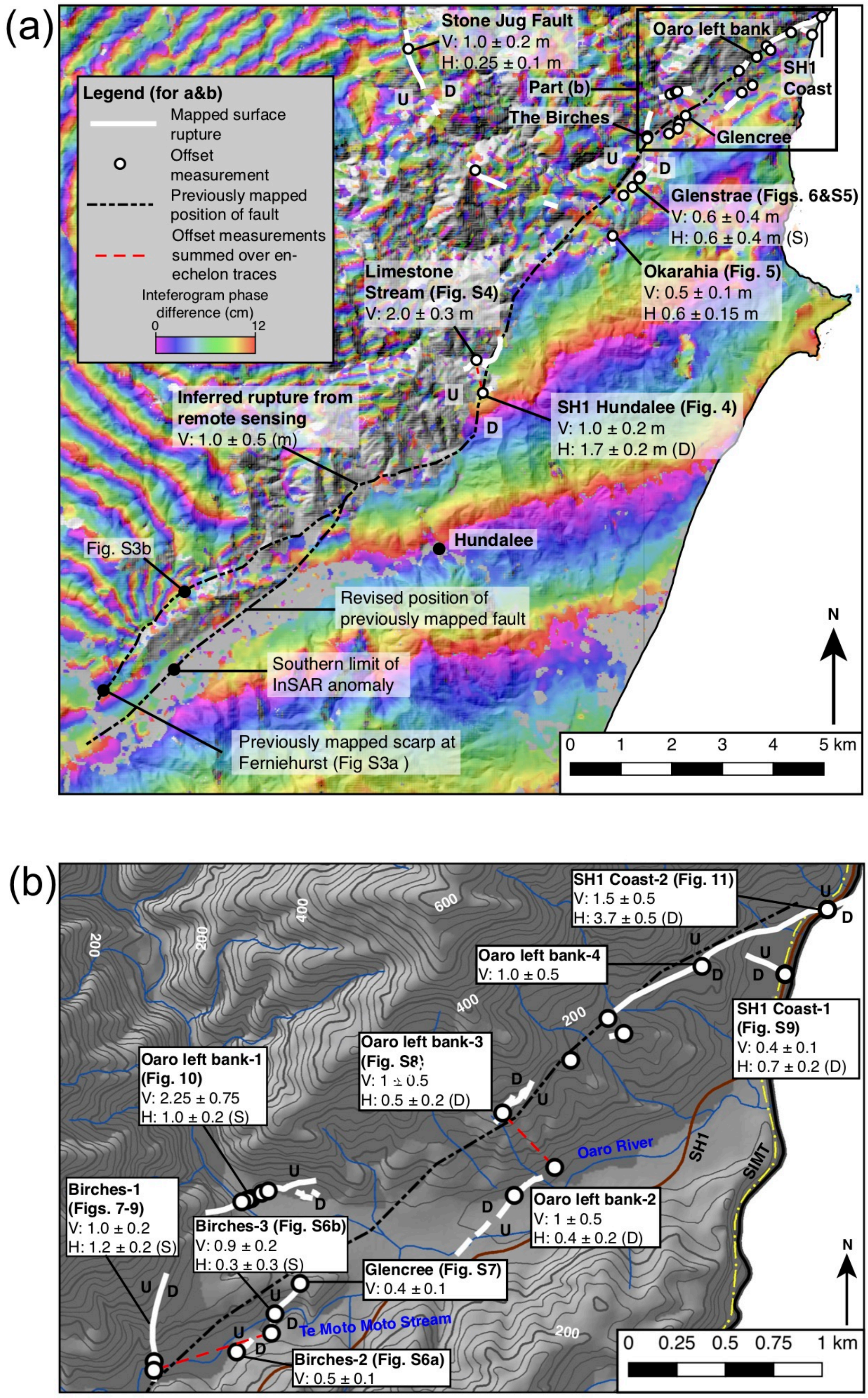

Figure 3: Surface ruptures along the Hundalee Fault that were formed by the 2016 Kaikōura Earthquake. (a) Overview map of all documented ruptures, underlain by an ascending ALOS-2

interferogram previously documented in Hamling et al., (2017). Extent of area shown in Fig. 2. The previously mapped position of the fault is derived from the QMAP dataset (Rattenbury et al., 2006) and the revised section of the fault is as shown in Fig. 2. These are used in the Hundalee Fault slip distribution plots (Fig. 12). (b) Map demonstrating the highly segmented and non-planar surface ruptures at the northeastern end of the Hundalee Fault. Note the differing sense of strike-slip and dip-slip displacement. In both figure parts, dashed lines indicate transects across which the offset measurements of en-echelon traces have been summed in Fig. 12c. The full range of offset measurements are given for each locality, for individual offset measurements see Table 1. V, vertical offset; H, horizontal offset; (S) and (D) = sinistral and dextral shear sense, U and D = upthrown and downthrown sides of the fault respectively; SH1, State Highway 1; SIMT: South Island Main Trunk Railway. Hillshade for both parts is derived from the Land Information New Zealand (LINZ) 8 m New Zealand Digital Elevation Model illuminated from the northwest. Topographic contours in (b) are at 20 m intervals (thicker lines, 100 m).

Figure 4

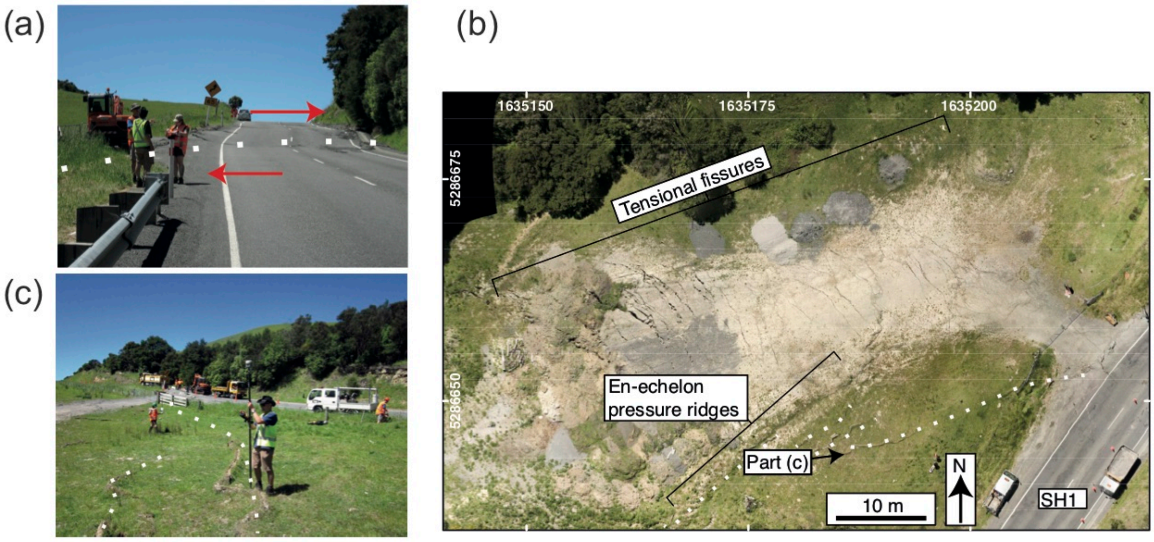

Figure 4: View northeast along State Highway 1 (SH1), 21 November 2016, at the SH1 Hundalee site (Fig. 3a), ~3 km north of Hundalee. (a) The Hundalee Fault has obliquely offset the road carriageway by 1.7 ± 0.2 m dextrally (arrows), and 1.0 ± 0.2 m up to the northeast. (b) Orthophoto of surface ruptures (white lines) in paddock on the southwest side of SH1, adjacent to the SH1 Hundalee site, derived from photos taken by UAV. Coordinates in New Zealand Transverse Mercator (NZTM). Location and perspective of part c also indicated. (c) View east-northeast towards the SH1 Hundalee offset, 22 November 2016, showing sinuous compressional turf rolls (white lines) in the foreground, resulting from Hundalee Fault surface rupture.

Figure 5

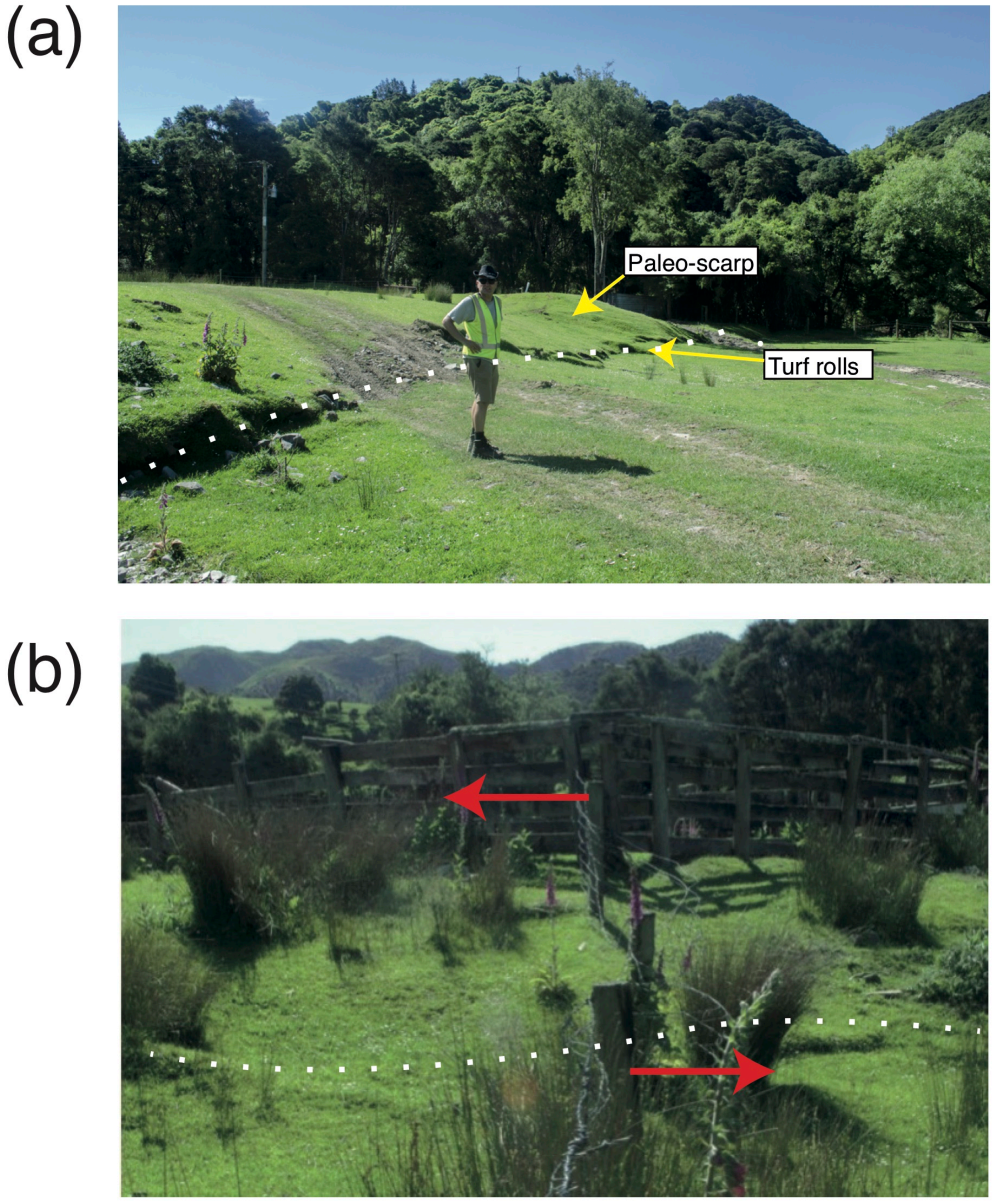

Figure 5: Surface ruptures at the Okarahia locality (Fig. 3a). (a) Dotted white line identifies 2016 surface rupture, characterized by a 0.5 ± 0.1 m high scarp with prominent turf rolls, taken 23 November 2016 looking west. A suspected pre-existing fault scarp at this location is evident in the background. (b) Sinistral-reverse offset (arrows) of 0.6 ± 0.15 m of a fence that crosses the scarp (dotted white line) at a high angle and results in dilation of the fence. Photo taken looking northwest.

Figure 6

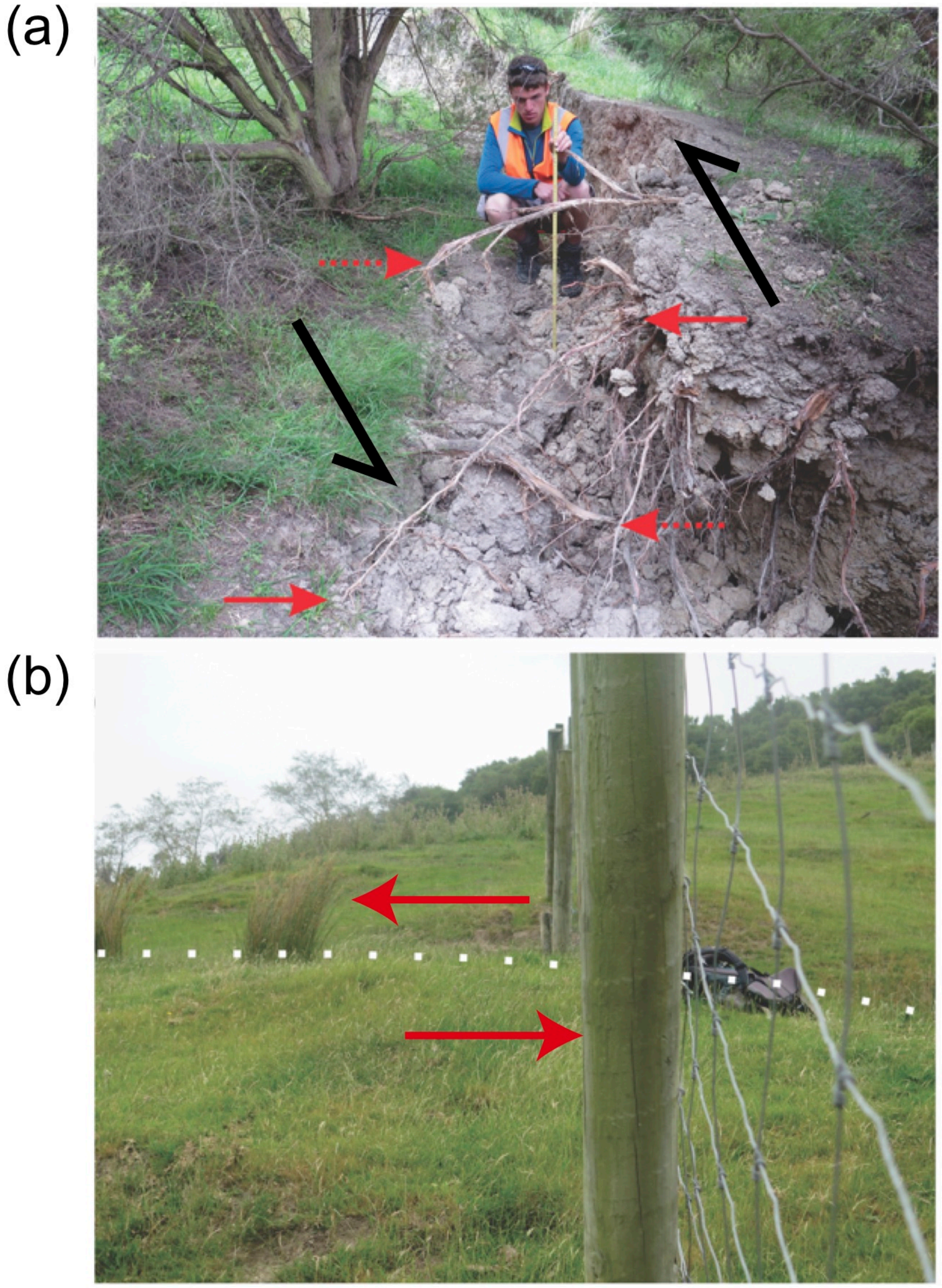

Figure 6: (a) Looking southwest at the 2016 rupture through a strand of trees along the Glenstrae locality (northernmost Glenstrae site; Fig. 3a, Table 1), 20 December 2016. We matched the ruptured ends of a large root (dashed arrow), and a small root was stretched but not broken (solid arrows). Both markers demonstrated a sinistral shift of 0.9 ± 0.1 m as shown by shear sense indicators. (b) Telephoto view southeast across the fault scarp (dotted white line) looking along a fence at the southern end of the Glenstrae sector (Fig. 3a, Table 1), 20 December 2016. The scarp is ~0.3 m high,

with a sinistral component of 0.2 ± 0.1 m recorded by the fence post offset. This is the smallest offset we were able to measure accurately on the Hundalee Fault.

Figure 7

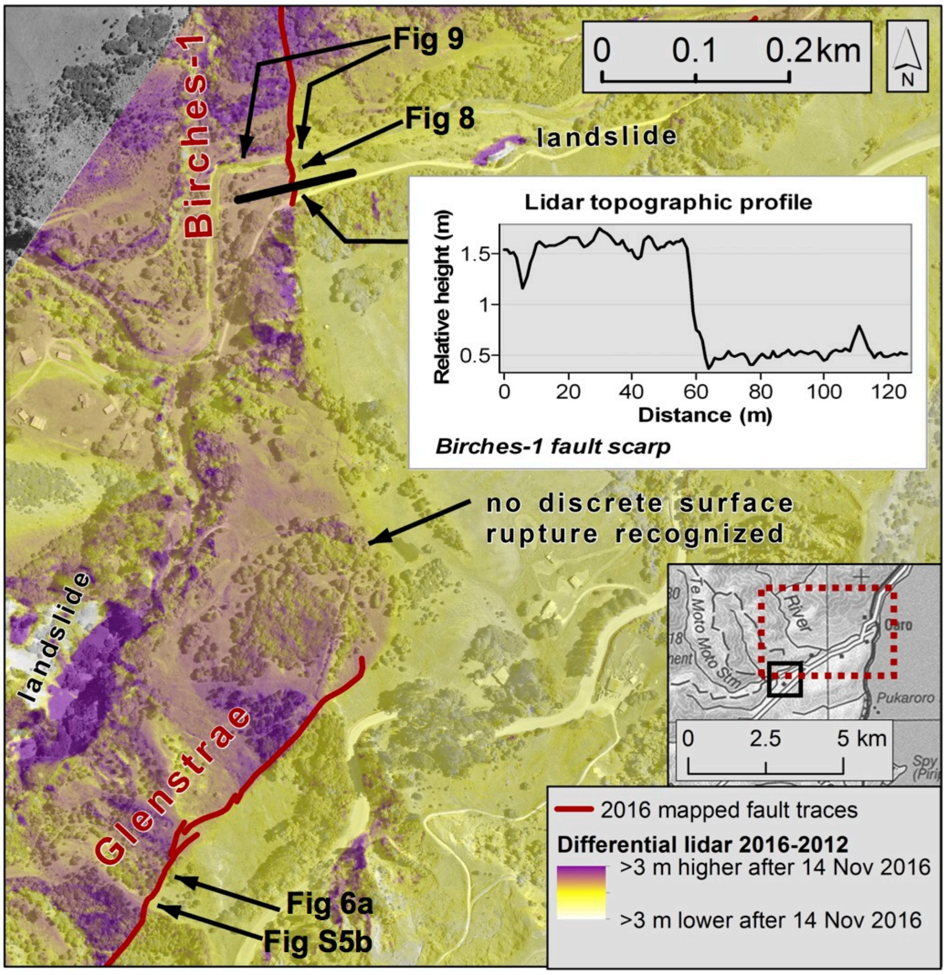

Figure 7: A continuation of 2016 surface rupture between The Birches and Glenstrae localities as revealed by differential lidar. The background image is the post-earthquake aerial photo mosaic at 0.2 m pixel resolution, rendered in greyscale and captured during the 2016 lidar acquisition flight. This is overlain transparently with a lidar differencing model, derived from a digital elevation model (DEM) generated from lidar acquired in 2012 that was subtracted from a DEM generated from post-earthquake lidar (Clark et al., 2017). The 2016 fault mapping is based on GPS surveying, and supplemented by identification of ruptured ground in the post-earthquake imagery. The reference to 14 Nov 2016 in the legend is for simplicity and assumes that all the elevation change occurred co-seismically; though we cannot exclude the possibility that some may have occurred in the time interval between the two lidar acquisition flights. Inset map shows area covered by this diagram (solid

box) in relation to Fig. 3b outline (dashed box). Profile through lidar differencing model is also shown (height relative to 2012 model) and was used to estimate vertical offset at Birches-1 (Table 1).

Figure 8

(a)

(b)

Figure 8: (a) View west towards the Birches-1 fault trace across low-level terrace on the south bank of Te Moto Moto Stream (Fig. 3b), 20 December 2016. Minimal soil development suggests the terrace surface is at most a few hundred years old. (a) the steep, vegetated, bank (white dotted line) down to the active stream channel (out of sight to right) has a sinistral offset of 1.1 ± 0.2 m across the fault (arrows), and the vertical component is also 1.1 ± 0.2 m. (b) The ruts of a vehicle track (arrows

marking right-hand rut) 30 m south of the photo (a) scene clearly illustrates the oblique sinistral and up-to-west shift.

Figure 9

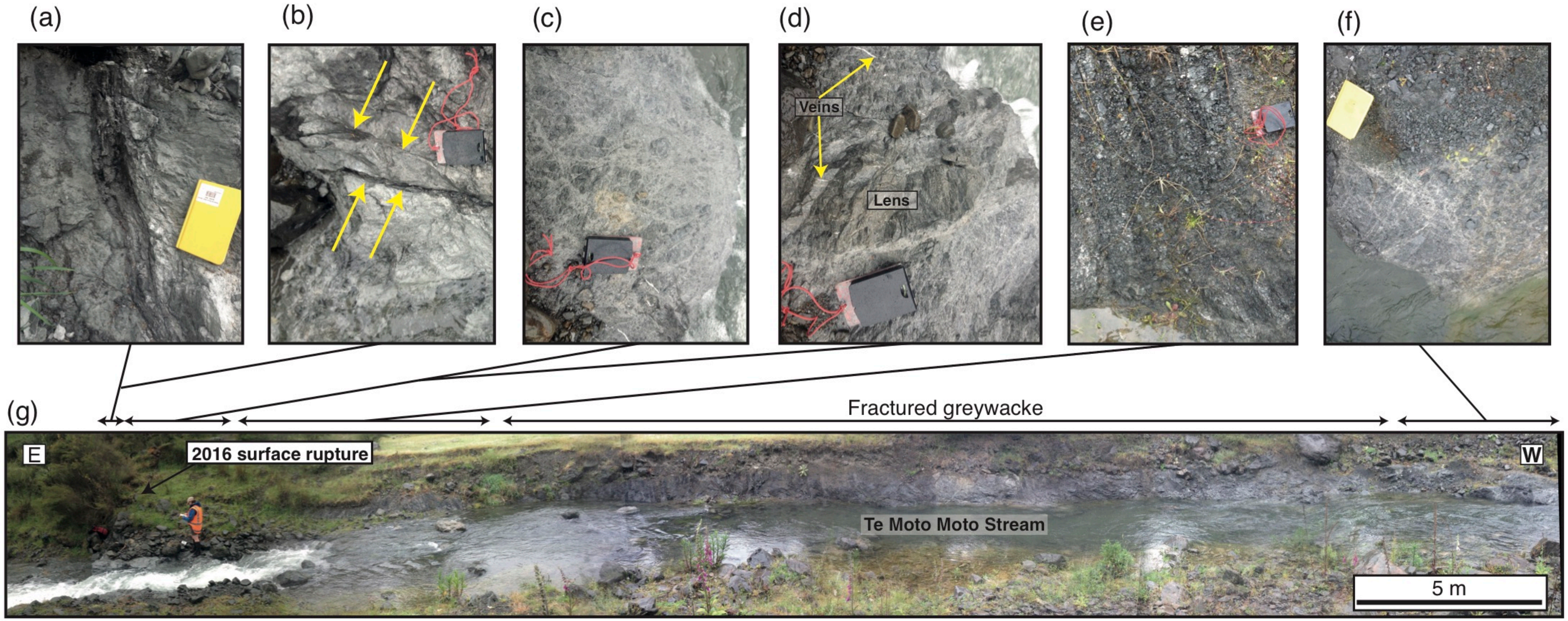

Figure 9: Bedrock exposure of the Hundalee Fault at Birches-1 locality. (a) <10 cm thick gouge which is located close to the 2016 surface rupture. (b) Thinner subsidiary gouge-filled fractures. (c-d) Greywacke derived breccia that comprises the fault zone within 5 m of the surface rupture. (e) Heavily fractured greywacke that lies up-section from the greywacke but in which the original bedding is still visible. (f) Localized zone of fault breccia located at western end of exposure, which may constitute a secondary strand of the Hundalee Fault and that does not show any surface rupture from the Kaikōura Earthquake. (f)

Entire exposed fault rock sequence of the Hundalee Fault along the Te Moto Moto stream, constructed from stitched images. Entire fault-rock sequence is >60 m thick. Length of compass clinometer is 8 cm and notebook is 20 cm respectively

Figure 10

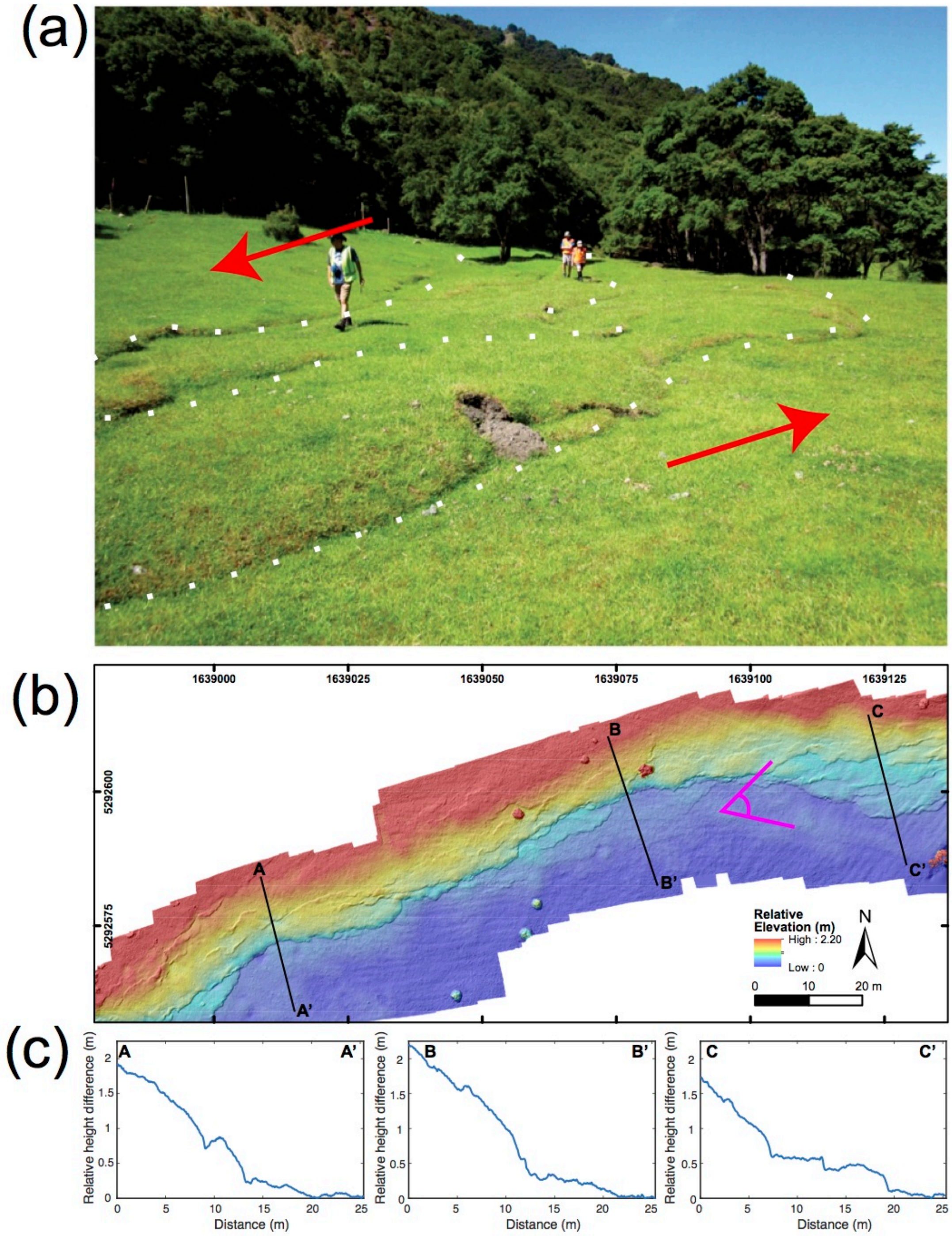

Figure 10: (a) View east-northeast along the Oaro Left Bank-1 fault scarp, ~200 m northeast of the Oaro River channel, showing multiple distributed rupture traces (dotted white lines), taken 22 November 2016. Up-to-the-northwest throw is accompanied by a subordinate sinistral component, identified from a fence-line offset (not shown, see Fig. S1, available in the electronic supplement to this article). Although ~10 m above river level, the flipped turf in the foreground reveals a very

immature soil developed on angular greywacke fine gravel, quite unlike the sub-rounded greywacke pebble bedload of the Oaro River. This terrace is interpreted to be a landslide dam-break aggradation fan, no more than a few hundred years old. (b) Digital elevation model (DEM) of surface ruptures at the Oaro Left Bank-1 locality, constructed from UAV derived photogrammetry model. The two lines with an angle symbol in between, indicates part (a) field of view. Map projection is NZTM/NZGD2000 Datum. (c) Three profiles through the DEM, with letters corresponding to transects indicated in part (b). These illustrate the distributed ground deformation and warping across at >20 m wide zone. Relative height differences should be regarded as a minimum as profiles are too narrow to cover the entire width of the deformation zone.

Figure 11

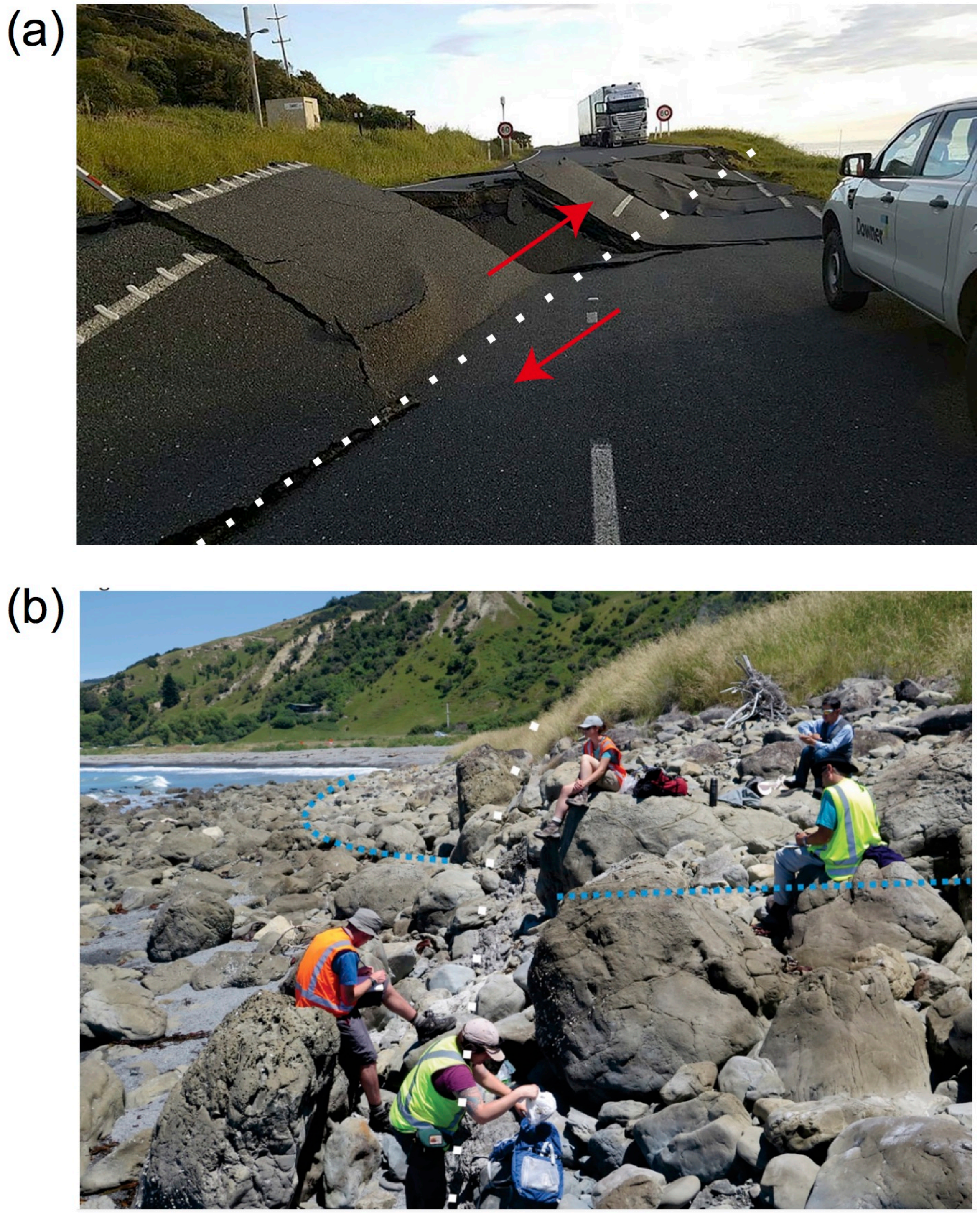

Figure 11: (a) Rupture (dotted white line) and uplift of State Highway 1 (SH1) at the coast (SH1 Coast-2 locality, Fig. 3b) where the maximum amount of onshore displacement (3.7 ± 0.5 m dextral, 1.5 ± 0.5 m vertical) was measured across the Hundalee Fault. Photo taken November 14, 2016 and supplied by the NZ Transport Agency. (b) View WSW along the fault scarp (white dotted line) across the beach face north of Oaro, near the SH1 Coast-2 locality, taken 21 December 2016. The vertical

movement, up to the NNW (right), as measured at SH1, is 1.5 ± 0.5 m. The closely-spaced dots denote an approximate a line of equal elevation on the pre-earthquake shoreface, above which the rocks are bleached, and highlight the lateral and vertical shift across the fault. In the foreground, mapping team members are sampling fault gouge exposed on the uplifted side of the fault.

Figure 12

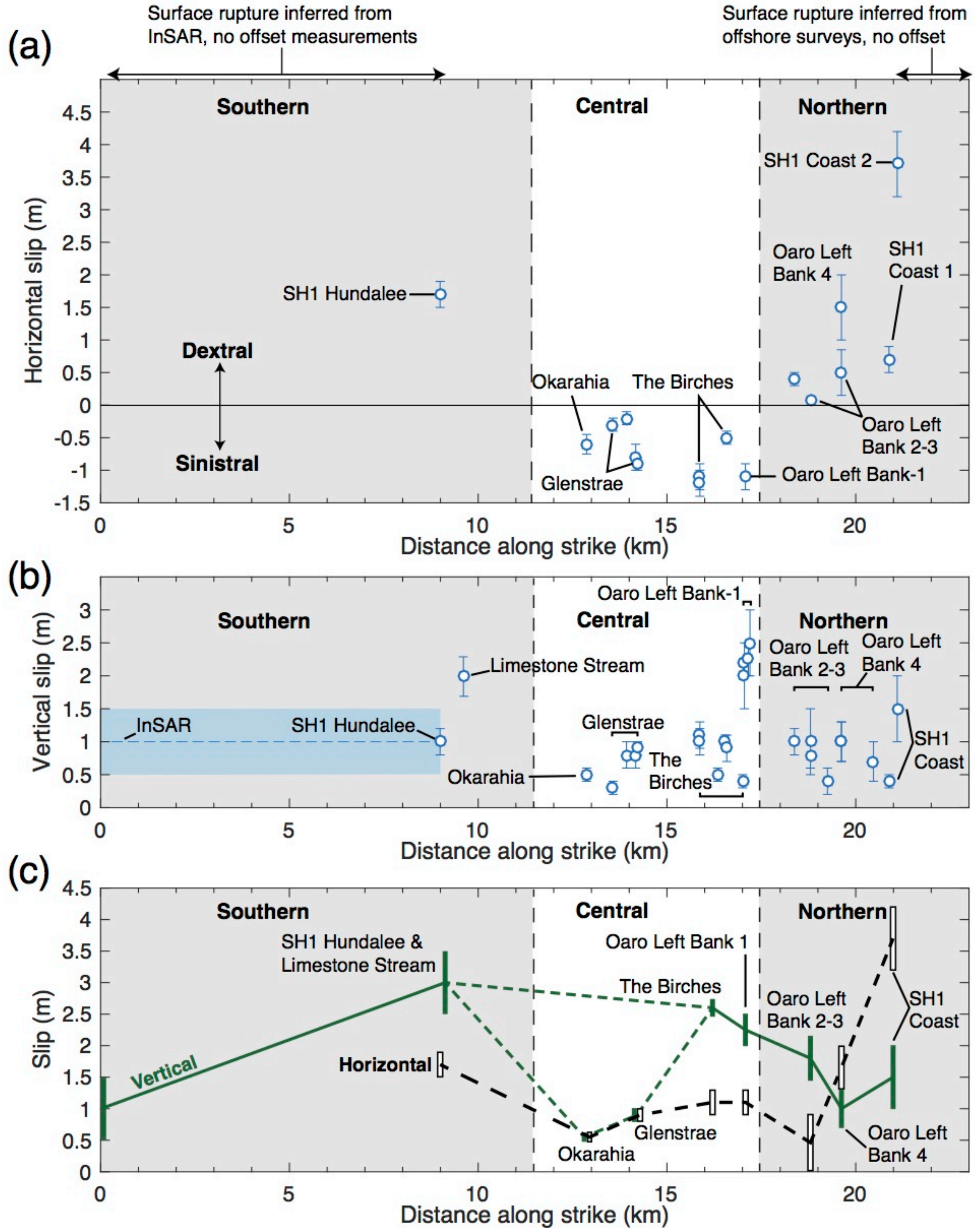

Figure 12: Slip distribution along the Hundalee Fault for (a) horizontal and (b) vertical offset using measurements listed in Table 1. Offset measurements are plotted against the previous mapped trace of the fault (Fig. 3; Warren, 1995; Rattenbury et al., 2006), and are projected onto it if necessary. InSAR is used to estimate vertical displacement along the fault's southern section in part (b), with the

uncertainties represented by the shaded region (Hamling et al., 2017). In (c), offset measurements are aggregated over *en-echelon* traces (SH1 Hundalee and Limestone Stream; The Birches 1 to 3; Oaro Left Bank 2 and 3), with a single representative measurement shown for all other localities to provide clarity. Dashed line for vertical slip in (c) for the Okarahia and Glenstrae localities highlights the anomalously low slip here recorded here and questions whether slip may have been distributed across another *en-echelon* trace that we did not find. Definition of southern, central, and northern sections illustrated in Fig. 13

Figure 13

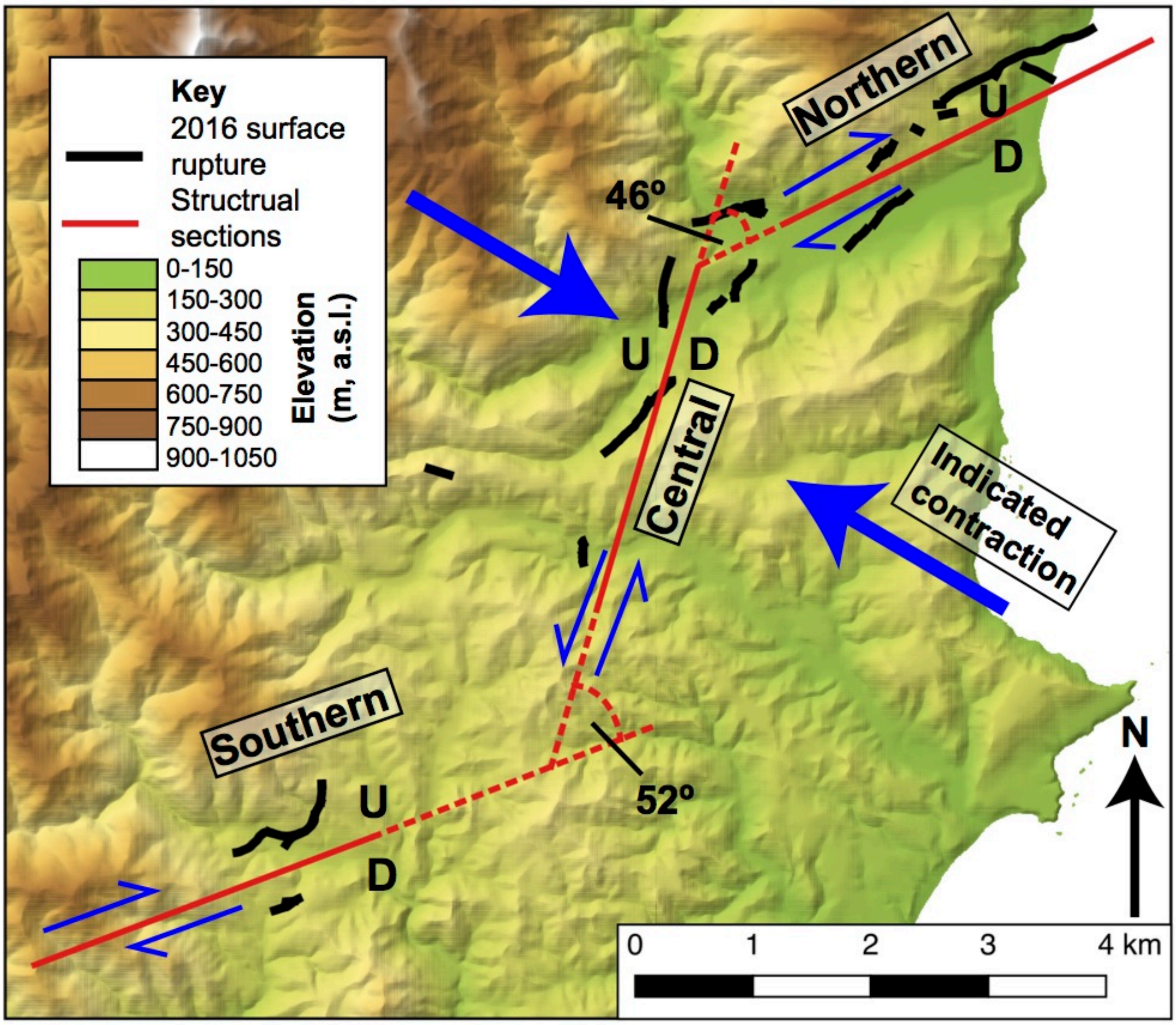

Figure 13: Division of the Hundalee Fault into southern and northern sections with east-northeast trending surface ruptures and a central section with north to north-northeast trending surface ruptures. Thick arrows represent contraction direction along an axis of 120°, which is required for the dextral shear sense observed along the northern and southern sections of the Hundalee Fault and sinistral shear sense along the central section. Note the northern-most surface rupture along the central section (Oaro Left Bank-1) is inconsistent with this interpretation. The interior angles between these sections are also shown. Lines are dashed where the end of these sections are projected. U and D = upthrown and downthrown sides of the fault respectively; m, meter; a.s.l., above sea level